

A deep survey of heavy element lines in Planetary Nebulae – I. Observations and forbidden-line densities, temperatures and abundances

Y. G. Tsamis^{1,2}, M. J. Barlow¹, X.-W. Liu^{1,3}, I. J. Danziger⁴ and P. J. Storey¹

¹Department of Physics and Astronomy, University College London, Gower Street, London WC1E 6BT, UK

²Met. Office, London Road, Bracknell RG12 2SZ, UK

³Department of Astronomy, Peking University, Beijing 100871, P.R. China

⁴Osservatorio Astronomico di Trieste, Via G. B. Tiepolo 11, I-34131 Trieste, Italy

Received:

ABSTRACT

We present deep optical spectrophotometry of twelve Galactic planetary nebulae (PNe) and three Magellanic Cloud PNe. Nine of the Galactic PNe were observed by scanning the spectrograph's slit across the nebula, yielding relative line intensities for the entire nebula that are suitable for comparison with integrated nebular fluxes measured in other wavelength regions. In this paper we use the fluxes of collisionally excited lines (CELs) from the nebulae to derive electron densities and temperatures, and ionic abundances. We find that the nebular electron densities derived from optical CEL ratios are systematically higher than those derived from the ratios of the infrared (IR) fine-structure (FS) lines of [O III]. The latter have lower critical densities than the typical nebular electron densities derived from optical CELs, indicating the presence of significant density variations within the nebulae, with the infrared CELs being biased towards lower density regions.

We find that for several nebulae the electron temperatures obtained from [O II] and [N II] optical CELs are significantly affected by recombination excitation of one or more of the CELs. When allowance is made for recombination excitation, much better agreement is obtained with the electron temperatures obtained from optical [O III] lines. We also compare electron temperatures obtained from the ratio of optical nebular to auroral [O III] lines with temperatures obtained from the ratio of [O III] optical lines to [O III] IR FS lines. We find that when the latter are derived using electron densities based on the [O III] 52 μm /88 μm line ratio, they yield values that are significantly higher than the optical [O III] electron temperatures. In contrast to this, [O III] optical/IR temperatures derived using the higher electron densities obtained from optical [Cl III] $\lambda\lambda 5517/\lambda 5537$ ratios show much closer agreement with optical [O III] electron temperatures, implying that the observed [O III] optical/IR ratios are significantly weighted by densities in excess of the critical densities of both [O III] FS lines. Consistent with this, ionic abundances derived from [O III] and [N III] FS lines using electron densities from optical CELs show much better agreement with abundances derived for the same ions from optical and ultraviolet CELs than do abundances derived from the FS lines using the lower electron densities obtained from the observed [O III] 52 μm /88 μm ratios. The behaviour of electron temperatures obtained making use of the temperature-insensitive [O III] IR FS lines provides no support for significant temperature fluctuations within the nebulae that could be responsible for derived Balmer jump electron temperatures being lower than temperatures obtained from the much more temperature sensitive [O III] optical lines.

Key words: ISM: abundances – ISM: lines – planetary nebulae: general

1 INTRODUCTION

This is the first of two papers devoted to the study of elemental abundances in a sample of Galactic and Magellanic Cloud

planetary nebulae which, together with a companion paper by Tsamis et al. (2003c; Paper II), focus on the problem of the optical recombination-line emission from heavy element ions (e.g. C²⁺, N²⁺, O²⁺) in planetary nebulae (PNe) and H II regions. The main manifestation of this intriguing question is the observed discrepancy between nebular elemental abundances derived from weak, optical recombination lines (ORLs; such as C II λ 4267, N II λ 4041, O II $\lambda\lambda$ 4089, 4650) on the one hand and the much brighter collisionally-excited lines (CELs; often collectively referred to as forbidden lines) on the other (Liu et al. 1995, 2000, 2001b; Tsamis 2002; Tsamis et al. 2003a), with ORLs typically being found to yield ionic abundances that are factors of two or more larger than those obtained from CELs emitted by the same ions. A closely linked problem involves the observed disparity between the nebular electron temperatures derived from the traditional [O III] (λ 4959 + λ 5007)/ λ 4363 ratio and the H I Balmer discontinuity diagnostic: the latter yields temperatures that are in most cases lower than those derived from the [O III] ratio (Peimbert 1971; Liu & Danziger 1993; Liu et al. 2001b; Tsamis 2002).

Tsamis et al. (2003a) have presented new spectroscopic observations and an abundance analysis of the Galactic H II regions M 17 and NGC 3576 and the Magellanic Cloud H II regions 30 Doradus, LMC N11B and SMC N66, involving both CELs and ORLs. We reported surprisingly large ORL vs. CEL abundance discrepancies in these objects: the O²⁺/H⁺ abundance ratios derived from multiple O II ORLs were found to be higher than the corresponding values derived from [O III] CELs, typically by a factor of ~ 2 , though for one nebula, LMC N11B, a factor of five discrepancy was found.

In the present paper, we present deep, long-slit, optical spectrophotometry of 12 Galactic and 3 Magellanic Cloud PNe. We present an extensive list of all the detected emission lines, including the numerous C II, N II, O II and Ne II ORLs, along with their fluxes and dereddened intensities. We undertake a *forbidden-line* abundance study deriving C, N, O, Ne, S, Cl and Ar abundances from CELs, as well as He abundances from He I and He II ORLs. Along with the optical data, we analyze *International Ultraviolet Explorer* NEWSIPS spectra of 10 PNe, which yield fluxes of important C, N, O and Ne CELs. We further derive abundances for a number of PNe from the far-IR [O III] 52- and 88- μ m and [N III] 57- μ m fine-structure lines using the *Infrared Space Observatory* LWS line fluxes by Liu et al. (2001a), as well as from the *IRAS* [Ne III] 15.5- μ m line fluxes by Pottasch et al. (1984). In an accompanying paper (Tsamis et al., Paper II), heavy-element ionic abundances are derived from the observed C II, C III, C IV, N II, N III, O II and Ne II ORLs and an extensive comparison between ORL and CEL elemental abundance ratios is made.

In Section 2 we describe our optical spectroscopic observations obtained with the ESO 1.52-m and NTT 3.5-m telescopes, as well as the data reduction process, and present emission line fluxes for all the PNe; we also present *IUE* ultraviolet (UV) observations and our data analysis methods. In Section 3 we describe the corrections for interstellar extinction to the UV and optical data. In Section 4 we present derived nebular electron temperatures and densities. In Section 5 we present our derived He/H ratios and the heavy element abundances derived from UV, optical and infrared (IR) collisionally-excited lines.

2 OBSERVATIONS

2.1 Optical spectroscopy

2.1.1 Description and data reduction

The planetary nebulae studied in this work were observed at the European Southern Observatory (ESO), using the 1.52-m telescope for the Galactic objects and the 3.5-m New Technology Telescope (NTT) for the Magellanic Cloud objects. The long-slit observations were taken during July and December 1995, July 1996 and February 1997. An observational journal is presented in Table 1.

The Boller & Chivens (B & C) spectrograph was used on the 1.52-m telescope in July 1995, equipped with a Ford 2048 \times 2048 pixel CCD detector, with each pixel $15\mu\text{m} \times 15\mu\text{m}$ in size. This detector was superseded in 1996 and 1997 by a UV-enhanced Loral 2048 \times 2048, $15\mu\text{m} \times 15\mu\text{m}$ CCD of improved quantum efficiency. A 2 arcsec wide, 3.5 arcmin long-slit was employed. During all runs the CCDs were binned by a factor of 2 along the slit direction, in order to reduce the read-out noise, yielding a spatial sampling of 1.63 arcsec per pixel projected on the sky. A 2400 lines per mm grating was used in first order, along with an order-sorting WG360 filter, to cover the 3995–4978 \AA wavelength range at a spectral resolution of 1.5 \AA FWHM. A second grating in first order, along with a WG345 filter, was used to cover the 3535–7400 \AA range at a resolution of 4.5 \AA (excluding NGC 2440 for which 4.5 \AA resolution spectra were not obtained). For three objects (NGC 5882, NGC 6302 and NGC 6818) an extra wavelength range (3040–4040 \AA) was covered with the holographic 2400 lines per mm grating at a resolution of 1.5 \AA , so that the high-order H I Balmer lines—transitions $n \rightarrow 2$, from upper levels of principal quantum number up to $n = 24$ —were accurately recorded. The low resolution (4.5 \AA), wider spectral coverage spectra, yielded fluxes of forbidden lines of N⁺, O⁺, O²⁺, Ne²⁺, S⁺, S²⁺, Cl²⁺, Ar²⁺ and Ar³⁺ etc. ions, as well as H⁰, He⁰ and He⁺ lines, and covered the Balmer discontinuity (or Balmer jump; BJ). The higher resolution (1.5 \AA), deep spectra recorded the optical recombination lines of C II, C III, C IV, N II, N III, O II and Ne II, the majority of which lay between 4000–5000 \AA .

Typical exposure times for these Galactic PNe ranged between 20 sec and 35 min. The short exposures were carefully chosen so that strong nebular lines, such as H α , H β or the [O III] $\lambda\lambda$ 4959, 5007 and [N II] $\lambda\lambda$ 6548, 6584 lines, would not be saturated. On the other hand, the deep exposures were aimed at capturing the faint ORLs, whose typical intensities can be as low as 10^{-4} that of H β , at an appropriate resolving power.

For nine out of twelve observed Galactic nebulae (NGC entries 2022, 2440, 3132, 3242, 3918, 5315, 5882 and IC 4191 and 4406) mean spectra were obtained by uniformly scanning the long-slit of the B&C spectrograph across the nebular surfaces (IC 4406 was scanned only at a lower resolution of 4.5 \AA). For these nebulae total fluxes of all detected lines can be derived, when total nebular H β line fluxes are adopted from the compilation of Cahn, Kaler & Stanghellini (1992; hereafter CKS92), as listed in column 2 of Table 1. Furthermore, these mean spectra are directly comparable with UV and IR spectra obtained from space-borne facilities (such as the *IUE*, *IRAS* and *ISO* satellites), whose large apertures usually capture most or all of the nebular emission, depending on the angular size of the observed nebulae and the pointing coordinates of such observations. In this way, several ionization stages of the same element can be traced, al-

lowing a more complete picture to be drawn for properties such as reddening, excitation class and elemental abundances.

For the remaining three Galactic PNe, plus IC 4406 in the 3995–4978 Å range only, fixed-slit spectra were obtained (Table 1). In those cases, the slit was positioned through the nebular center – using the central star of the PN as a guide, if visible – and passing through the visually brightest parts of the nebula.

The Magellanic Cloud planetary nebulae LMC N66, LMC N141 and SMC N87 were observed at ESO with the 3.5-m NTT, in December 1995 (Table 1). The ESO Multi-Mode Instrument (EMMI) was used in the following modes: red imaging and low dispersion grism spectroscopy (RILD), blue medium dispersion spectroscopy (BLMD) and dichroic medium dispersion spectroscopy (DIMD). The detector was a TEK 1024 × 1024, 24 μm × 24 μm CCD (no. 31; on the blue arm), used while in BLMD observing mode and a TEK 2048 × 2048, 24 μm × 24 μm CCD (no. 36; on the red arm), while in RILD mode. Both cameras were in use when observing in DIMD mode. In those cases, a dichroic prism is inserted into the beam path so that light is directed to the blue and red grating units in synchronization, allowing simultaneous exposures to be obtained in the blue and red parts of the optical spectrum. For all exposures, both CCDs were binned by a factor of 2 in both directions, in order to reduce the read-out noise. The spatial sampling was thus 0.74 and 0.54 arcsec per pixel projected on the sky, for CCDs no. 31 and no. 36, respectively.

Four wavelength regions were observed with two different gratings (#3, #7) at spectral resolutions of approximately 2 Å FWHM (3635–4145, 4060–4520, 4515–4975 Å), and 3.8 Å (6507–7828 Å), respectively. An extra wavelength range, 3800–8400 Å, was covered only for LMC N66 at a resolution of 11 Å, using a grism (#3). An OG530 filter was used when observing in DIMD mode. The slits used were 5.6 arcmin long and 1 and 1.5 arcsec wide, but wide-slit 5 arcsec grism observations were also taken for LMC N66. Exposure times for the Magellanic Cloud PNe ranged from 3 to 30 min.

The two-dimensional Galactic PN spectra were reduced with the LONG92 package within MIDAS. They were bias-subtracted, flat-fielded via division by a normalized flat field, cleaned of cosmic-rays, and then wavelength-calibrated using exposures of a He-Ar calibration lamp. The effect of atmospheric extinction was removed by correcting the spectra using extinction coefficients for the La Silla site. During the 1997 run, twilight sky flat-fields were also obtained with the purpose to correct the small variations in illumination along the slit, which were ∼1–3 per cent. For the 1995 and 1996 runs, the spectra were flux-calibrated using wide-slit (8 arcsec) observations of the *HST* standard stars Feige 110 and the nucleus of the PN NGC 7293 (Walsh 1993). The flux distributions of the standards were modeled with high-order spline fits. In 1997, the CTIO standard stars LTT 4363, LTT 6248 (Hamuy et al. 1994) and the *HST* standard HD 49798 (Walsh 1993) were used.

The 3040–4040 Å spectra of NGC 5882, 6302 and 6818 are affected by ozone absorption bands, shortwards of 3400 Å (Schachter 1991). The bands have a typical width of ∼15 Å, i.e. much wider than the nebular emission lines (∼1.5 Å). In order to remove the ozone absorption we used the ozone-opacity template derived by Liu et al. (2000) for the study of NGC 6153 from the same site (ESO, La Silla) as the observations presented herein. The standard stars Feige 110 and the nucleus of NGC 7293 were observed with a narrow 2 arcsec slit, i.e. the same as the one used for nebular observations. These narrow-slit

spectra were used to derive the ozone opacity per unit airmass as a function of wavelength, relative to the mean atmospheric extinction curve at La Silla. The opacity curve, scaled by the airmasses of the nebular exposures, was then used to divide out the ozone absorption bands.

The Cloud PN two-dimensional spectra were reduced with similar procedures as above; the wavelength calibration was done with respect to Th-Ar and He-Ar calibration lamps within MIDAS, while flux calibration was performed with respect to wide-slit (8 arcsec) observations of the standard Feige 110, within the IRAF package.

For all flux-calibrated spectra suitable sky windows were selected on each side of the nebular emission, their increments were summed-up, scaled to the total number of CCD pixels along the slit direction and subtracted. In this way we were able to subtract the sky emission for all PNe, since their angular diameters were always effectively contained within our long-slit. The resulting spectra were subsequently averaged along the spatial nebular emission—defined by the extent of the H β line—to yield the one-dimensional spectra on which our nebular analysis was performed. In a couple of cases, such as NGC 6302 and NGC 6818 for which only fixed-slit spectra were obtained, the ORLs detected were rather weak and the spectra slightly noisier than the norm, so we decided to integrate the spectra along the spatial extent of the C II λ4267 line which is one of the strongest heavy element recombination lines in nebulae (the H β line was of course sampled over the same pixel numbers). This resulted in better S/N ratios for the O II and N II recombination lines too, which are expected to originate from similar nebular volumes as the C II λ4267 line.

In other objects it was found that light from the nebula's central star affects considerably the nebular line fluxes or the shape of the observed continuum spectrum. For instance, NGC 3132 harbours a binary nucleus whose primary component is the A-type star HD 87892 (Kohoutek & Laustsen 1977; Sahu & Desai 1986). The absorption line spectrum of this star affects severely the nebular Balmer lines by diminishing their intensities, so a few central CCD pixels had to be excluded from the integration in order to prevent such contamination and to restore the nebular line profiles. Another example is NGC 5882 which possesses a weak emission line ('wel'), hydrogen-deficient nucleus, whose continuum energy distribution evidently affects the shape of the nebular continuum in the region of the Balmer discontinuity (∼3646 Å). Thus in order to get an accurate measurement of the Balmer jump intensity and the high-order Balmer lines from the deep 3040–4040 Å spectra of this object, we again excluded several central pixels when averaging the two-dimensional CCD frames. This restored the nebular continuum to its expected shape at those wavelengths.

In Fig. 1 we show a representative high resolution optical spectrum of NGC 3242 taken in scanning mode. It is a time-weighted average of four deep exposures which captured a particularly rich set of recombination lines from heavy element ions. Indicative line identifications are shown; they can be found in full in Table 3.

2.2 The IUE observations

We complemented our optical dataset with *IUE* ultraviolet observations of 10 of the Galactic PNe, together with *IUE* observations of the 3 Magellanic Cloud nebulae; the remaining two

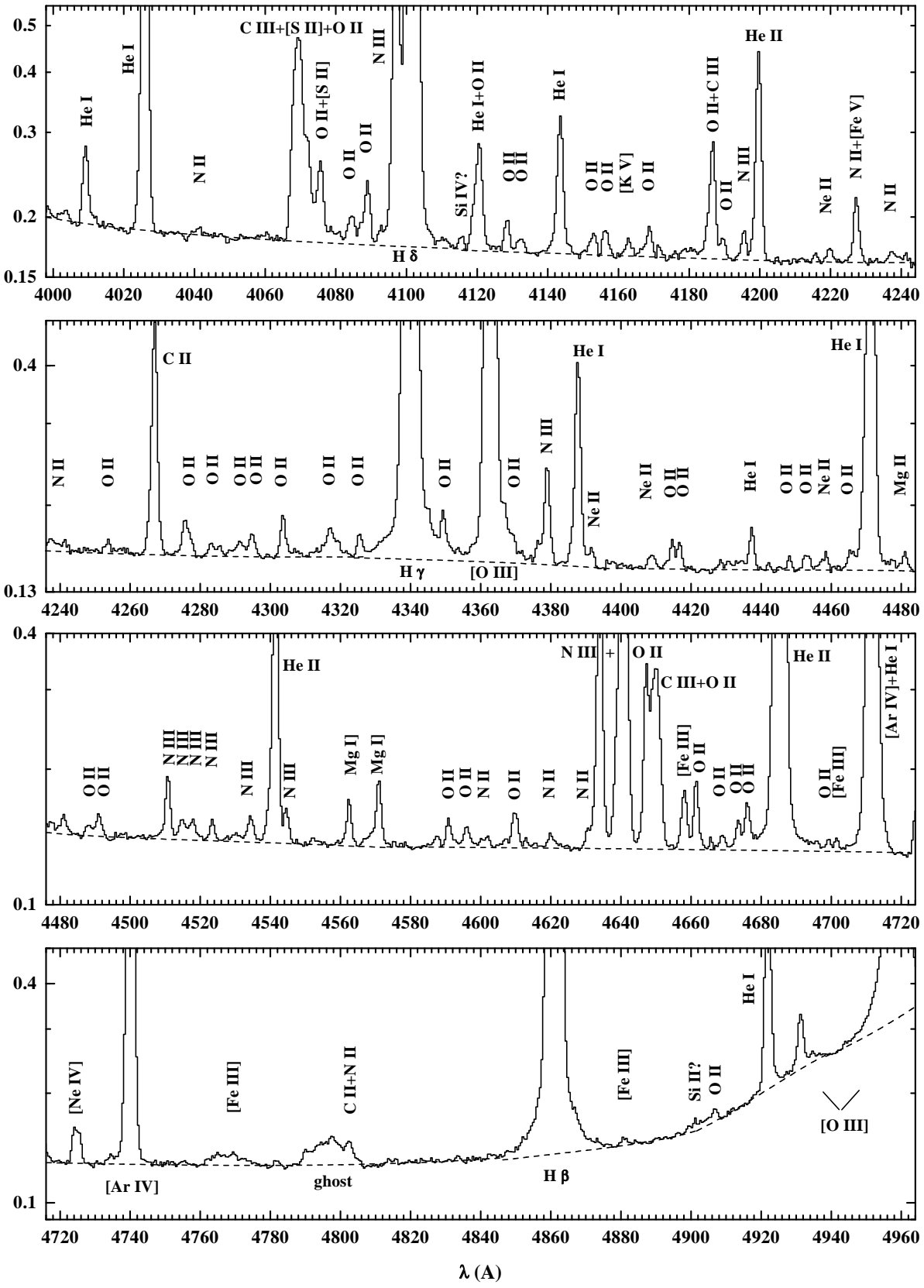


Figure 1. The spectrum of NGC 3242 from 4000 to 4960 Å featuring the prominent recombination lines from C, N, O and Ne ions; it was obtained by uniformly scanning the entire nebular surface using a narrow long-slit. The dashed lines show the adopted continuum level. The steep rise of the continuum after 4880 Å is an instrumental artifact. The intensity is in units such that $F(H\beta) = 100$; the spectrum is not corrected for interstellar extinction.

Table 1. Journal of ESO optical observations.

PN	$\log F(\text{H}\beta)$ (ergs cm^{-2} s^{-1})	$c(\text{H}\beta)^{\text{radio}}$	Date (UT)	λ -range (Å)	FWHM (Å)	Mode	Exp. Time (sec)
<u>ESO 1.52-m</u>							
NGC 2022	−11.13	0.42	7 Feb 1997	3530–7428	4.5	scanning	40, 1155
			8, 10 Feb 1997	3994–4978	1.5	"	3 × 1500, 1800, 2100
NGC 2440	−10.50	0.47	9 Feb 1997	3994–4978	1.5	scanning	1800
NGC 3132	−10.45	0.30	7 Feb 1997	3530–7428	4.5	scanning	70, 1147
			8, 10 Feb 1997	3994–4978	1.5	"	2 × 1620, 2 × 1800
NGC 3242	−9.79	0.17	7 Feb 1997	3530–7428	4.5	scanning	25, 480
			8, 10 Feb 1997	3994–4978	1.5	"	1614, 2 × 1800, 2100
NGC 3918	−10.04	0.40	7 Feb 1997	3530–7428	4.5	scanning	20, 22, 40, 200
			8, 10 Feb 1997	3994–4978	1.5	"	1020, 1200, 2 × 1620
NGC 5315	−10.42	0.55	7 Feb 1997	3530–7428	4.5	scanning	30, 240
			9, 10 Feb 1997	3994–4978	1.5	"	1080, 1350, 2 × 1500
NGC 5882	−10.38	0.42	12 Jul 1996	3040–4050	1.5	fixed slit	2 × 1800
			7 Feb 1997	3530–7428	4.5	scanning	20, 220
			9, 10 Feb 1997	3994–4978	1.5	"	3 × 1500, 1800
NGC 6302	−10.55	1.39	11 Jul 1996	3040–4050	1.5	fixed slit	2 × 1800
			29 Jul 1995	3530–7428	4.5	"	30, 60, 300
			23 Jul 1995	3994–4978	1.5	"	3 × 1800
NGC 6818	−10.48	0.37	11 Jul 1996	3040–4050	1.5	fixed slit	2 × 1800
			29 Jul 1995	3530–7428	4.5	"	60, 300
			23 Jul 1995	3994–4978	1.5	"	3 × 1800
IC 4191	−10.99	0.70	7 Feb 1997	3530–7428	4.5	scanning	2 × 30, 500
			8 Feb 1997	3994–4978	1.5	"	900, 1200
			29 Jul 1995	3530–7428	4.5	fixed slit	5, 10, 300, 600
IC 4406	−10.75	0.27	22 Jul 1995	3994–4978	1.5	"	3 × 1800
			7 Feb 1997	3530–7428	4.5	scanning	50, 1080
			29 Jul 1995	3530–7428	4.5	fixed slit	2 × 300
My Cn 18	−11.21	0.74	22 Jul 1995	3994–4978	1.5	"	5 × 1800
			29 Jul 1995	3530–7428	4.5	fixed slit	2 × 120, 600
			23 Jul 1995	3994–4978	1.5	"	4 × 1800
<u>NTT 3.5-m</u>							
SMC N87	−12.48		17 Dec 1995	6507–7828	3.8	fixed slit	1200
			"	3635–4145	2	"	1200
			"	4060–4520	2	"	2 × 1800
			"	4515–4975	2	"	900, 3 × 1800
LMC N66	−12.68		17 Dec 1995	3800–8400	11	fixed slit	2 × 300
			"	6507–7828	3.8	"	300
			"	3635–4145	2	"	300
			"	4060–4520	2	"	360
			"	4515–4975	2	"	600
LMC N141	−12.48		17 Dec 1995	6507–7828	3.8	fixed slit	1200
			"	3635–4145	2	"	1800
			"	4060–4520	2	"	2 × 1800
			"	4515–4975	2	"	180, 4 × 1800

Galactic PNe, IC 4191 and My Cn 18, were never observed by the *IUE*. Low-resolution, large aperture spectra obtained with the SWP and LWP cameras were accessed via the Space Telescope Science Institute's website. The wavelength coverage of the two cameras is 1150–1975, and 1910–3300 Å, respectively. All observations were obtained with the *IUE* large aperture, a 10.3×23 arcsec 2 oval. The data were retrieved in final (NEWSIPS) calibrated form. When several spectra for one object were available, they were co-added weighted by the integration time. The employed *IUE* exposures are listed in Table 2. For NGC 3918 the line fluxes reported by Clegg et al. (1987) were used, combined with those retrieved from a more recent expo-

sure (SWP 47514). Similarly, in the analysis of NGC 5315 and NGC 6818 we used the line fluxes recently listed by Feibelman (1998; see his Table 3) and by Hyung, Aller & Feibelman (1999; see their Tables 4 and 5), respectively. Regarding LMC N66, we used the observed *IUE* line fluxes listed by Pena & Ruiz (1988; from spectrum SWP 19905).

The apparent angular sizes of all nebulae in our sample, apart from NGC 5315 and the Magellanic Cloud nebulae, are larger than the *IUE* large aperture. Thus, in most cases only a certain fraction of the UV nebular emission was captured by the satellite. This delicate aspect of the observations is discussed in the following Section.

Table 2. Journal of *IUE* observations.^a

PN	Spectrum	Exp. Time (sec)
NGC 2022	SWP 32732, 32729	4800, 5400
NGC 2440	SWP 07264, 14850, 17243	1800, 2100, 360
	SWP 32720	2400
NGC 3132	SWP 06160, 01745, 49629	7200, 1200, 7200
NGC 3242	SWP 5154, 5155	300, 330
NGC 3918	SWP 47514	300
NGC 5882	SWP 16349	1800
NGC 6302	SWP 05210, 05211	720, 5400
	SWP 30986, 33379	14400, 6600
IC 4406	SWP 23420, 36237	3600, 7200
	LWP 03725, 15490	3600, 7200
SMC N87	LWR 10043, SWP 13387	10500, 13387
LMC N141	SWP 13408	9000

^a NGC 5315 and NGC 6818 line fluxes were taken from Feibelman (1998) and Hyung et al. (1999) respectively; for NGC 3918 the combined fluxes from SWP 47514 and those of Clegg et al. (1987) were used.

2.3 Data analysis

With respect to the optical data we proceeded by normalizing the individual one-dimensional spectra to a flux scale such that $F(H\beta) = 100$, in order to merge them afterwards. When $H\beta$ was found to be saturated in one spectrum, the scaling was achieved using a suitable unsaturated H I Balmer line from a shorter duration exposure. The 3040–4040 Å Galactic PN spectra were brought to scale with the rest, using emission lines detected in common with the 3535–7400 Å spectra, such as H I $\lambda 3835$, [Ne III] $\lambda 3868$, H I + He I $\lambda 3889$, and [Ne III] $\lambda 3967$ + He I $\lambda 3970$. In a similar fashion, the Magellanic Cloud PN spectra from different grating settings were brought to scale via their overlapping portions. For two of them, SMC N87 and LMC N141, their 6507–7828 Å spectra had no overlap in wavelength with other grating settings. In this case we normalized the spectra to $F(H\beta) = 100$, using the theoretical intensity ratio $I(H\alpha)/I(H\beta) = 2.85$, a value predicted for representative nebular conditions of $T_e = 10000$ K and $N_e = 5000 \text{ cm}^{-3}$ (Storey & Hummer 1995); we also took into account the amount of reddening estimated towards these objects (Section 5). Finally, the normalized spectra taken at each grating setting were co-added, weighted by the exposure time, in order to achieve an optimum S/N ratio.

Regarding the UV data, a way had to be found to scale them to the normalized optical spectra. For all Galactic nebulae (except NGC 5315, NGC 6818 and IC 4406), we used the theoretical intensity ratio for He II $\lambda 1640/\lambda 4686$, calculated for the appropriate nebular temperatures and densities using the recombination theory predictions of Storey & Hummer (1995). In this way we scaled the UV spectra to $F(H\beta) = 100$ using our measurements of the dereddened $I(\lambda 1640)$ and $I(\lambda 4686)$ fluxes. In cases where the [O II] $\lambda 2470$ doublet line was detected, as in NGC 6818 and IC 4406, we used instead the predicted intensity ratio [O II] $(\lambda 7320 + \lambda 7330)/\lambda 2470 = 1.33$, which holds independently of nebular conditions since all lines involved arise from the same upper levels (A -values taken from Zeippen 1982). The method was found to be highly reliable; for instance in NGC 5315 whose angular diameter fits completely within the *IUE* large aperture—and there is thus no need for any aperture correction to be applied—the [O II] $\lambda 2470$ intensity predicted

using the optical [O II] $\lambda\lambda 7320, 7330$ intensities, is within 2 per cent of the actual UV measurement. For NGC 5315 and the three Cloud PNe (SMC N87, LMC N66 and LMC N141) the dereddened UV line fluxes were scaled directly to $F(H\beta) = 100$, with the use of total $H\beta$ fluxes from CKS92 in the former case and from those listed by Barlow (1987) in the latter cases.

We proceeded with measuring the emission line fluxes from the UV and optical spectra using the MIDAS package. First we scrutinized the low resolution *IUE* spectra in order to determine the nature of the emission lines, which in some cases can have a stellar and not nebular origin (e.g. N V $\lambda 1240$, C IV $\lambda 1550$, He II $\lambda 1640$). The FWHM of the lines was compared against that of *IUE* low resolution spectra which is $\sim 6\text{--}7$ Å. Lines with FWHM of $\gtrsim 8\text{--}9$ Å were checked for blending or for the possible presence of P Cygni features that would betray their origin in a central star's wind, as is the case for instance in NGC 5315 and NGC 5882.

Most of the line fluxes—and certainly all those of heavy element recombination lines—were derived using Gaussian line profile fitting techniques, apart from the strongest ones, for which their fluxes were measured by simply integrating over the lines. Gaussian line fitting within MIDAS is performed through least-squares fitting using the Newton-Raphson method.

Even in our 1.5 Å high-resolution optical spectra, blending of emission lines is evident throughout the wavelength range covered and it particularly affects weak features like the ORLs of interest. The line broadening is dominated by instrumental broadening and not by nebular dynamics, since the typical FWHM of 1.5 Å translates to $\sim 93 \text{ km s}^{-1}$ at 4861 Å, whereas typical PN expansion velocities are $\lesssim 25 \text{ km s}^{-1}$ (e.g. Kwock 1994). Therefore, in order to de-convolve features affected by blending, multiple Gaussian fitting was employed. In such cases a successful estimate of the continuum emission level was deemed to be a very important first step. After subtracting the local continuum, line fluxes were retrieved by fitting multiple Gaussians of appropriate central wavelength and usually equal FWHM. The FWHM was taken to be the same as that of nearby unblended lines of similar strength to the ones fitted. Their relative wavelength spacing was constrained to that from laboratory wavelengths. This procedure assured accurate flux retrieval and aided line identification in the case of ambiguous features.

In rare instances where the fitting process was not adequately yielding unique fluxes for closely spaced lines, we made use of the theoretical intensity ratios of selected lines, assuming *LS*-coupling to hold for the ions in question (e.g. Kuhn 1969). As an example, in PNe of relatively high excitation class, such as NGC 5882, the [S II] $\lambda 4068$ line is blended with the C III V 16 triplet, whose components at 4067.94, 4068.91, and 4070.26 Å have intensity ratios under pure *LS*-coupling of 1.00 : 1.31 : 1.71 (e.g. Allen 1973). Also present in this blend are the O II V 10 multiplet $\lambda\lambda 4069.62, .89$ and 4072.16 lines. We therefore fitted 6 Gaussians to the 4069 Å complex, fixing the C III triplet relative intensities according to theory, while allowing the intensities of the other lines to vary independently. After reducing by 2 the number of free parameters in the minimization problem, convergence was more readily achieved. Of course in this way, the resulting flux for the C III triplet refers to the sum of its components only, while information on the true allocation of flux among them is lost. Individual fluxes, however, are retrieved for the [S II] and O II lines and the overall shape of the blend is accurately reproduced (see Fig. 2). As another example, the blend at 4650 Å can be fitted with 5 Gaussians, includ-

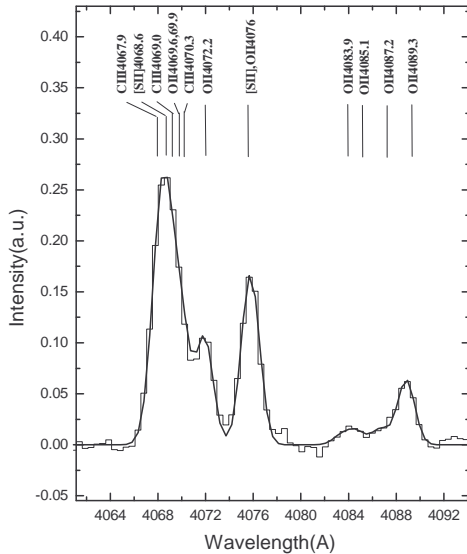


Figure 2. High resolution spectrum (1.5 Å FWHM) of NGC 5882: the blend of O II quartet V 10, C III triplet V 16 and [S II] doublet is well fitted by multiple Gaussians (thick line); also present are O II 4f–3d transitions of which $\lambda\lambda 4089.3$ ($J = 11/2-9/2$) is the strongest predicted line. See text for more details.

ing the O II $\lambda\lambda 4649.13, 4650.84$ lines from multiplet V 1 and the C III V 1 triplet $\lambda\lambda 4647.42, 4650.25$ and 4651.47 lines, the latter having relative intensities of 5 : 3 : 1 as predicted under LS-coupling. In general, apart for the aforementioned cases we avoided fixing the relative strengths of ORLs, since we were interested to compare our observations with the predictions of current recombination theory, especially for O II.

Table 3 presents the observed optical relative line intensities for the 12 Galactic PNe in our sample, while Table 4 presents the observed optical and ultraviolet relative line intensities for the 3 Magellanic Cloud PNe. Table 5 presents the ultraviolet nebular line intensities for the 10 Galactic PNe in the sample which were observed by the *IUE*. Typical optical line flux errors are estimated to be less than 5 per cent for lines with observed fluxes $F(\lambda) \geq 0.2$ [in units of $F(H\beta) = 100$], 10 per cent for those with $0.1 \leq F(\lambda) \leq 0.2$, 20 per cent for $0.05 \leq F(\lambda) \leq 0.1$, and 30 per cent or more for lines with $F(\lambda) \leq 0.05$. For a given flux range, the errors for optical lines shortwards of 3400 Å are slightly larger, due to the decreasing CCD efficiency towards the end of the spectral coverage and the effects of ozone absorption.

Table 3. Observed and dereddened relative line fluxes [$F(\lambda)$] and $I(\lambda)$, respectively], on a scale where $H\beta = 100$.

λ_{obs}	$F(\lambda)$	NGC 222			
		$c(H\beta)^{\text{Ba}} = 0.38$	ID	λ_0	Mult
*	*	[S III]	3721.63	F2	
*	*	H 14	3721.94	H14	
1.16(+1)	1.45(+1)	[O II]	3726.03	F1	
*	*	[O II]	3728.82	F1	
*	*	H 13	3734.37	H13	
3750.89	3.78	4.71	H 12	3750.15	H12
3757.98	2.80	3.48	?		
3760.61	2.62	3.26	O III	3759.87	V2
3771.37	4.14	5.13	H 11	3770.63	H11
3797.88	5.41	6.68	H 10	3797.90	H10
3815.06	7.94(-1)	9.78(-1)	?		
3835.37	7.17	8.80	H 9	3835.39	H9
3869.16	4.55(+1)	5.56(+1)	[Ne III]	3868.75	F1
3889.46	1.08(+1)	1.32(+1)	He I	3888.65	V2
3922.34	6.26(-1)	7.57(-1)	He II	3923.48	4.15
3967.88	2.65(+1)	3.18(+1)	[Ne III]	3967.46	F1
4025.99	1.34	1.59	He I	4026.21	V18
4041.28	4.92(-2)	5.80(-2)	N II	4041.31	V39b
4060.39	1.56(-1)	1.84(-1)	[F IV]	4060.23	
4068.47	3.70(-1)	4.35(-1)	C III	4067.87	V16
4069.57	4.84(-1)	5.70(-1)	C III	4068.97	V16
4070.90	6.32(-1)	7.44(-1)	C III	4070.30	V16
4072.76	2.69(-1)	3.16(-1)	O II	4072.16	V10
4076.46	2.50(-1)	2.94(-1)	O II	4075.86	V10
4090.02	1.72(-1)	2.02(-1)	O II	4089.29	V48a
4098.09	1.04	1.22	N III	4097.33	V1
4102.21	2.39(+1)	2.80(+1)	H 6	4101.74	H6
4119.75	7.15(-2)	8.34(-2)	O II	4119.22	V20
*	*	He I	4120.84	V16	
4122.71	1.80(-1)	2.09(-1)	O II	4121.46	V19
4143.97	1.74(-1)	2.02(-1)	He I	4143.76	V53
4163.78	1.26(-1)	1.46(-1)	[K V]	4163.30	F1
4185.98	8.17(-2)	9.40(-2)	O II	4185.45	V36
4187.43	2.88(-1)	3.32(-1)	C III	4186.90	V18
4200.42	1.79	2.06	He II	4199.83	4.11
4228.17	5.16(-1)	5.89(-1)	[Fe V]	4227.74	F2
4267.78	7.24(-1)	8.20(-1)	C II	4267.15	V6
4276.62	1.64(-1)	1.85(-1)	O II	4276.75	V67b
4341.00	4.58(+1)	5.11(+1)	H 5	4340.47	H5
4350.13	1.04(-1)	1.16(-1)	O II	4349.43	V2
4363.78	1.29(+1)	1.43(+1)	[O III]	4363.21	F2
4367.46	2.50(-1)	2.77(-1)	O II	4366.89	V2
4370.43	1.31(-1)	1.45(-1)	Ne II	4369.86	V56
4377.24	1.74(-1)	1.92(-1)	?		
4379.98	4.26(-1)	4.72(-1)	N III	4379.11	V18
4388.50	7.54(-2)	8.33(-2)	He I	4387.93	V51
4409.86	4.61(-2)	5.07(-2)	Ne II	4409.30	V55e
4415.46	1.14(-1)	1.25(-1)	O II	4414.90	V5
4435.13	5.89(-2)	6.44(-2)	N III	4434.14	V2
4449.43	6.97(-2)	7.61(-2)	O II	4448.19	V35
4453.61	2.60(-1)	2.83(-1)	?		
4459.36	1.49(-1)	1.62(-1)	?		
4472.10	6.33(-1)	6.87(-1)	He I	4471.50	V14
4476.25	8.62(-2)	9.35(-2)	O II?	4477.90	V88
*	*	Mg II	4481.21	V4	
4511.52	1.48(-1)	1.59(-1)	N III	4510.91	V3
4517.74	6.85(-2)	7.37(-2)	N III	4518.15	V3
4535.41	6.51(-2)	6.97(-2)	N III	4534.58	V3
4542.22	3.54	3.79	He II	4541.59	4.9
4571.37	4.23(-2)	4.49(-2)	Mg I]	4571.10	
4607.24	1.06(-1)	1.12(-1)	N IV	4606.33	
4610.33	5.47(-2)	5.78(-2)	O II	4609.44	V92a

3 INTERSTELLAR EXTINCTION

Before proceeding with any kind of formal analysis, nebular spectra have to be corrected for the effects of interstellar extinction caused by dust. In nebular studies the amount of interstellar reddening is most usually described by $c(\text{H}\beta)$, which is the logarithmic difference between observed and intrinsic (or else dereddened) $\text{H}\beta$ fluxes. The reddening-corrected nebular fluxes [in units of $I(\text{H}\beta) = 100$] are then given by

$$I(\lambda) = 10^{c(\text{H}\beta)f(\lambda)} F(\lambda),$$

where $f(\lambda)$ is the adopted extinction curve normalized such that $f(\text{H}\beta) = 0$.

A common way to derive $c(\text{H}\beta)$ in optical studies of nebulae is from a comparison between the observed and predicted H I Balmer decrement, using the $\text{H}\alpha/\text{H}\beta$, $\text{H}\gamma/\text{H}\beta$ and $\text{H}\delta/\text{H}\beta$ line ratios. This is the method we have adopted in order to deredden our optical spectra; three preliminary $c(\text{H}\beta)$ values were obtained from each of the above Balmer line ratios and then averaged with weights of 3 : 1 : 1, respectively, according to the wavelength separation of the lines. The comparison was against the theoretical ratios from Storey & Hummer (1995) for representative values of $T_e = 10000\text{ K}$ and $N_e = 5000\text{ cm}^{-3}$. Subsequent iteration, once the true nebular temperatures and densities were derived, resulted in negligible changes for $c(\text{H}\beta)$, denoted as $c(\text{H}\beta)^{\text{Ba}}$ hereafter. The reddening correction applied using $c(\text{H}\beta)^{\text{Ba}}$ effectively compensates for errors introduced by the relative flux calibration of the spectra. The main disadvantage over other methods is the relatively small wavelength separation of the Balmer lines employed. The values of $c(\text{H}\beta)^{\text{Ba}}$ that were used to deredden each optical spectrum are given in Tables 3 and 4 under the heading of each PN's line-list. The two values listed for IC 4406 correspond to the scanned and fixed-slit spectra, respectively.

A more accurate estimate of $c(\text{H}\beta)$ is possible through a comparison of the observed (optically thin) radio free-free continuum radiation of the PN, e.g. at 5 GHz, with the observed total $\text{H}\beta$ flux. Since the wavelength baseline involved is large and the radio flux suffers virtually no extinction, this method gives highly reliable reddening estimates and is to be preferred when global nebular properties are studied. In this way we derived reddening values for our Galactic PNe using the formulae of Milne & Aller (1975), employing total $\text{H}\beta$ and 5 GHz continuum fluxes taken from CKS92, along with He^+/H^+ and $\text{He}^{2+}/\text{H}^+$ fractions deduced from our optical observations (see Section 5.1). Similarly, one can also derive $c(\text{H}\beta)$ from a comparison between the $\text{He II } \lambda 1640$ and $\lambda 4686$ or $[\text{O II}] \lambda 2470$ and $\lambda \lambda 7320, 7330$ integrated line fluxes.

In this work we used the value of $c(\text{H}\beta)$ derived from the radio- $\text{H}\beta$ method, denoted $c(\text{H}\beta)^{\text{radio}}$ (as listed in column 3 of Table 1), to deredden the UV line fluxes in cases where the apparent PN diameter was larger than the *IUE* large aperture. All UV fluxes were then scaled to the optical spectra as described previously in Section 4. In our sample, apart from NGC 5315 and the Cloud nebulae, the PNe angular diameters are larger than the *IUE* large aperture, so the derived $c(\text{H}\beta)^{1640}$ values are consistently greater than the one given by $c(\text{H}\beta)^{\text{rad}}$, since the derivation involves a comparison between a fraction of the $\text{He II } \lambda 1640$ line flux with the total nebular $\text{He II } \lambda 4686$ flux; therefore $c(\text{H}\beta)^{1640}$ values were not used in our analysis.

The Magellanic Cloud PN spectra were dereddened in a two step process. First the contribution from Galactic fore-

Table 3. –continued

λ_{obs}	$F(\lambda)$	$I(\lambda)$	NGC 6302			
			$c(\text{H}\beta)^{\text{Ba}} = 1.44$	ID	λ_0	Mult
3118.22	1.16	5.24			*	
3120.54	1.31	5.86	O III	3121.71	V12	
3131.16	1.66	7.33	O III	3132.79	V12	
3184.38	1.21(−1)	4.96(−1)	Si III	3185.12	V8	
3187.00	8.32(−1)	3.38	He I	3187.74	V3	
3202.37	7.10	2.82(+1)	He II	3203.10	3.5	
3239.26	7.04(−2)	2.67(−1)		?		
3241.15	3.95(−1)	1.49	Si III	3241.62	V6	
3298.89	8.16(−1)	2.86	O III	3299.36	V3	
3311.83	2.27	7.87	O III	3312.30	V3	
3334.52	3.68(−2)	1.22(−2)	Ne II	3334.84	V2	
3340.26	3.73	1.24(+1)	O III	3340.74	V3	
3345.38	2.51(+1)	8.33(+1)	[Ne V]	3345.86		
3354.22	5.61(−2)	1.84(−1)		?		
3361.83	1.49(−1)	4.86(−1)	[Na IV]	3362.20		
3380.59	7.55(−2)	2.40(−1)	O IV	3381.21		
3384.90	5.80(−2)	1.83(−1)	O IV	3385.52		
3405.33	1.41(−1)	4.38(−1)		?		
3411.35	6.41(−2)	1.97(−1)	O IV	3411.69		
3414.92	2.67(−1)	8.21(−1)	O III	3415.31		
3425.45	7.69(+1)	2.33(+2)	[Ne V]	3425.86		
3429.65	6.25(−1)	1.88	O III	3428.65	V15	
3432.71	1.12(−1)	3.37(−1)		?		
3443.66	6.90	2.05(+1)	O III	3444.07	V15	
3466.13	4.04(−1)	1.17	He I	3467.54		
3478.27	6.33(−2)	1.81(−1)	He I	3478.97	V43	
3553.98	8.45(−2)	2.24(−1)	He I	3554.20	V34	
3567.92	8.19(−2)	2.14(−1)	Ne II	3568.50	V9	
3586.70	1.69(−1)	4.35(−1)	He I	3587.28	V31	
3613.18	1.20(−1)	3.02(−1)	He I	3613.64	V6	
3633.66	1.69(−1)	4.17(−1)	He I	3634.25	V28	
3671.16	7.20(−2)	1.73(−1)	H 24	3671.48	H24	
3673.38	1.40(−1)	3.37(−1)	H 23	3673.74	H23	
3676.03	2.00(−1)	4.81(−1)	H 22	3676.36	H22	
3678.99	2.60(−1)	6.25(−1)	H 21	3679.36	H21	
3682.46	3.10(−1)	7.43(−1)	H 20	3682.81	H20	
3686.46	3.90(−1)	9.33(−1)	H 19	3686.83	H19	
3691.18	4.50(−1)	1.07	H 18	3691.56	H18	
3696.81	6.50(−1)	1.54	H 17	3697.15	H17	
3703.62	1.20	2.84	H 16	3703.86	H16	
	*	*	He I	3705.02	V25	
3711.64	1.07	2.52	H 15	3711.97	H15	
3714.54	9.50(−2)	2.23(−1)	O III	3715.08	V14	
	*	*	H 14	3721.94	H14	
3721.14	2.11	4.96	[S III]	3721.63	F2	
3725.54	1.28(+1)	3.00(+1)	[O II]	3726.03	F1	
3728.33	6.00	1.40(+1)	[O II]	3728.82	F1	
3733.88	7.71(−1)	1.79	H 13	3734.37	H13	
3749.69	1.00	2.32	H 12	3750.15	H12	
3754.19	3.03(−1)	6.99(−1)	O III	3754.69	V2	
3756.74	2.24(−1)	5.16(−1)	O III	3757.24	V2	
3759.37	1.63	3.76	O III	3759.87	V2	
3770.17	1.25	2.86	H 11	3770.63	H11	
3773.31	3.63(−2)	8.26(−2)	O III	3774.02	V2	
3777.81	3.79(−3)	8.54(−2)	Ne II	3777.14	V1	
3781.28	5.90(−2)	1.33(−1)	He II	*		
3790.86	8.03(−2)	1.81(−1)	O III	3791.27	V2	
3797.46	1.78	4.00	H 10	3797.90	H10	
3805.53	2.48(−2)	5.54(−2)	He I	3805.74	V58	
3813.12	9.30(−2)	2.06(−1)	He II	3813.50	4.19	
3819.27	4.97(−1)	1.10	He I	3819.62	V22	
3834.98	2.85	6.27	H 9	3835.39	H9	
3839.10	2.32(−2)	5.07(−2)	[Fe V]	3839.27		
3855.83	1.49(−1)	3.22(−1)	?			

data. The SMC extinction law of Prevot et al. (1984) was used in the case of SMC N87, while the mean LMC extinction law of Howarth (1983) was used for LMC N141. For the directions to SMC N87 and LMC N141, $c(\text{H}\beta) = 0.03$ and 0.11 through the Milky Way were found respectively. From the foreground-corrected Balmer decrements, values of $c(\text{H}\beta) = 0.02$ and 0.03 , respectively, were found for the remaining Magellanic Cloud extinction. For LMC N66, the observed optical Balmer line ratios were already consistent with Case B values, so no extinction correction was applied to the optical line fluxes. We corrected the observed *IUE* line fluxes of Pena & Ruiz (1988) by comparing the observed He II $\lambda 1640/\lambda 4686$ flux ratio of 5.1 with the theoretical Case B value of 7.4 for $T_e = 2 \times 10^4$ K. This yielded $c(\text{H}\beta) = 0.14$ (0.09 Galactic; 0.05 LMC), which was applied to deredden the UV line fluxes.

Another kind of correction had to be applied for high-excitation objects with a high He II $\lambda 4686$ flux [e.g. $\gtrsim 65$ when $F(\text{H}\beta) = 100$]; in such nebulae the He II Pickering series (transitions $n \rightarrow 4$) begins to contribute significantly to the H I Balmer series. Relevant cases include NGC 2022, NGC 2440, NGC 6302 and LMC N66, where the contribution to $\text{H}\beta$ from He II Pi 8 was estimated using the observed He II $\lambda 4686$ flux and emissivities from Storey & Hummer (1995). Fluxes of the contaminating He II $\lambda 4859$ ($n = 8 \rightarrow 4$) amounted to $\sim 3\text{--}5$ per cent and were subtracted from the $\text{H}\beta$ fluxes before any further analysis was performed.

Throughout the above analysis we used total nebular $F(\text{H}\beta)$ and 5 GHz continuum fluxes for the Galactic PNe, as listed by CKS92; from them total nebular He II $\lambda 4686$ fluxes were derived, using the observed $I(\lambda 4686)/I(\text{H}\beta)$ ratios from our scanned nebular spectra. In the case of nebulae that were observed only with a fixed-slit we proceeded as follows: for NGC 6302 we used the total nebular He II flux from CKS92 directly, without resorting to our fixed-slit $I(\lambda 4686)/I(\text{H}\beta)$ ratio, while for NGC 6818 the above optical ratio was assumed to be representative of the whole PN.

4 NEBULAR DIAGNOSTICS

Nebular electron temperatures and densities were derived from several CEL diagnostic ratios by solving the equations of statistical equilibrium for multi-level (≥ 5) atomic models using the program EQUIB (originally written by I.D. Howarth and S. Adams). The following diagnostic ratios were used:

$$\begin{aligned} T_e(\text{O III}): & I(\lambda 4959 + \lambda 5007)/I(\lambda 4363) \\ T_e(\text{O III})_{\text{IR}}: & I(\lambda 4959 + \lambda 5007)/I(52\mu\text{m} + 88\mu\text{m}) \\ T_e(\text{N II}): & I(\lambda 6548 + \lambda 6584)/I(\lambda 5754) \\ T_e(\text{O II}): & I(\lambda 3727)/I(\lambda 7320 + \lambda 7330) \\ T_e(\text{S II}): & I(\lambda 4068)/I(\lambda 6731 + \lambda 6716) \\ T_e(\text{BJ}): & I_c(\lambda 3646^- - \lambda 3646^+)/I(\text{H} 11) \\ N_e(\text{Ar IV}): & I(\lambda 4740)/I(\lambda 4711) \\ N_e(\text{Cl III}): & I(\lambda 5537)/I(\lambda 5517) \\ N_e(\text{S II}): & I(\lambda 6731)/I(\lambda 6716) \\ N_e(\text{O II}): & I(\lambda 3729)/I(\lambda 3726) \end{aligned}$$

The procedure to derive temperatures and densities from CEL line ratios is as follows: we assumed a representative initial electron temperature of 10000 K to derive $N_e(\text{Cl III})$ and $N_e(\text{Ar IV})$. We then used the mean density from these diagnostics to derive $T_e(\text{O III})$ and iterated once to get the final values. In a similar manner, $T_e(\text{N II})$ was derived in conjunction with

$N_e(\text{O II})$ and $N_e(\text{S II})$. The atomic data used for the purpose of this analysis, but also throughout this work, are those used by Liu et al. (2000) in their case study of NGC 6153.

4.1 Electron Densities

The derived electron densities for our sample of PNe are listed in Table 6. In all spectra the [Ar IV] $\lambda 4711$ line is blended with the He I $\lambda 4713$ line; individual fluxes for the two lines were thus derived by means of Gaussian profile fitting, as described previously in Section 6. Both of the [Ar IV] $\lambda\lambda 4711, 4740$ fluxes were measured on high-resolution spectra (1.5 Å for the Galactic PNe and 2 Å for the Magellanic Cloud PNe) in all cases; they were then used to derive the $N_e(\text{Ar IV})$ values listed in Table 6.

We were able to derive N_e 's using the [O II] $\lambda 3729/\lambda 3726$ ratio only for NGC 5882, 6302 and 6818, for which the [O II] $\lambda\lambda 3726, 3729$ doublet was resolved in the high-resolution $3040\text{--}4040$ Å spectra. For the remaining PNe the [O II] doublet is covered in lower resolution only and is blended with the H I $\lambda 3721.9$, [S III] $\lambda 3721.6$ and H I $\lambda 3734.4$ lines; the overall [O II] flux was derived as follows: the [S III] $\lambda 3721$ flux was estimated from a comparison with the dereddened flux of the [S III] $\lambda 6312.1$ line, which originates from the same upper level. The latter line is often blended with He II $\lambda 6310.8$ in high excitation objects and that flux was retrieved via its theoretical ratio relative to He II $\lambda 4686$. Finally, the $I(\text{H} 13)/I(\text{H}\beta)$ and $I(\text{H} 14)/I(\text{H}\beta)$ intensity ratios were estimated using H I line emissivities from Storey & Hummer (1995). The deconvolved $\lambda 3727$ flux was then used to derive N_e 's for the remaining PNe of Table 6 from the [O II] $I(\lambda 3727)/I(\lambda 7320 + \lambda 7330)$ ratio.

Electron densities were also derived from the [O III] $52\mu\text{m}/88\mu\text{m}$ ISO LWS line flux ratios measured for eight of our sample PNe by Liu et al. (2001a)¹.

It should be borne in mind that the derived densities correspond to mean values, since the employed line ratios have been taken from scanned nebular spectra in most cases. In addition, all observations sampled lines of sight throughout the nebular volumes as well. It is thus quite probable that localized density variations on a small scale have been effectively smoothed out, or that they are not even seen due to the relatively low spatial resolution of our observations.

On the other hand, the $N_e(\text{S II})$ values for the whole sample are consistently lower than the $N_e(\text{Ar IV})$ values, by about ~ 30 per cent. This behaviour is consistent with the presence of strong density variations in the nebulae, so that the diagnostic line ratios with higher critical densities (e.g. the [Cl III] and [Ar IV] diagnostics) yield higher derived nebular electron densities.² The effect is shown to be more pronounced from a comparison between the [O III] $52\mu\text{m}/88\mu\text{m}$ and [Cl III] and [Ar IV] densities. For the eight PNe for which values from all three of these ratios have been derived, the latter diagnostics yield N_e 's that are on average a factor of 6 higher than those ob-

¹ Liu et al. adopted a constant electron temperature of 10^4 K to derive electron densities from their $52\mu\text{m}/88\mu\text{m}$ flux ratios and compared their values to those derived from the [Cl III] and [Ar IV] optical doublet ratios.

² [Cl III] $\lambda\lambda 5517, 5537$, $N_{\text{cr}} = 6400, 34000 \text{ cm}^{-3}$; [Ar IV] $\lambda\lambda 4711, 4740$, $N_{\text{cr}} = 14000, 130000 \text{ cm}^{-3}$; [S II] $\lambda\lambda 6716, 6730$, $N_{\text{cr}} = 1200, 3300 \text{ cm}^{-3}$ respectively.

Table 5. *IUE* fluxes of Galactic PNe.^a

Line	NGC 2022		NGC 2440		NGC 3132		NGC 3242		NGC 3918	
	$F(\lambda)$ (10^{-14})	$I(\lambda)$ $c = 0.55$	$F(\lambda)$ (10^{-13})	$I(\lambda)$ $c = 0.52$	$F(\lambda)$ (10^{-13})	$I(\lambda)$ $c = 0.33$	$F(\lambda)$ (10^{-13})	$I(\lambda)$ $c = 0.20$	$F(\lambda)$ (10^{-12})	$I(\lambda)$ $c = 0.40$
N V $\lambda 1240$	*	*	28.3	105	*	*	*	*	6.70	41.1
O IV] $\lambda 1401$	47.8	124	21.3	52.9	*	*	*	*	10.8	48.9
N IV] $\lambda 1486$	38.3	90.1	82.2	186	*	*	*	*	11.0	46.4
C IV $\lambda 1549$	367	814	309	659	49.3	7.40	*	*	113	458
[Ne V] $\lambda 1574$	9.78	21.3	5.83	12.2	*	*	*	*	*	*
[Ne IV] $\lambda 1601$	6.94	14.8	*	*	*	*	*	*	1.50	5.90
He II $\lambda 1640$	378	790	255	514	17.8	25.9	890	172	73.3	284
O III] $\lambda 1663$	8.58	17.7	19.6	39.2	2.08	3.00	43.9	8.50	8.20	31.5
N III] $\lambda 1750$	*	*	70.6	140	3.18	4.60	28.7	5.50	7.00	26.7
C III] $\lambda 1908$	224	526	410	924	26.4	41.1	741	150	117	493
Line	NGC 5315		NGC 5882		NGC 6302		NGC 6818		IC 4406	
	$F(\lambda)^c$ (10^{-13})	$I(\lambda)$ $c = 0.57$	$F(\lambda)$ (10^{-13})	$I(\lambda)$ $c = 0.43$	$F(\lambda)$ (10^{-13})	$I(\lambda)$ $c = 1.47$	$F(\lambda)^e$ (10^{-12})	$I(\lambda)$ $c = 0.36$	$F(\lambda)$ (10^{-13})	$I(\lambda)$ $c = 0.30$
N V $\lambda 1240$	*	*	*	*	3.01	1382	7.90	15.9	*	*
O IV] $\lambda 1401$	3.54	.679	*	*	1.46	112	21.5	32.6	*	*
N IV] $\lambda 1486$	1.95	2.58	*	*	6.96	534	22.2	31.6	*	*
C IV $\lambda 1549$	*	*	*	*	8.39	552	70.8	96.7	4.84	19.9
[Ne V] $\lambda 1574$	6.21	7.41	*	*	*	*	7.30:	9.84:	*	*
[Ne IV] $\lambda 1601$	2.06	2.41	*	*	0.30 ^d	26.6	5.20	6.94	*	*
He II $\lambda 1640$	*	*	15.3	17.8	7.24	409	242	318	21.0	83.8
O III] $\lambda 1663$	3.9	4.42	4.25	4.90	2.34	129	22.8	29.8	1.97	7.80
N III] $\lambda 1750$	4.7	5.26	3.90	4.50	7.61	408	16.4	21.2	1.99	7.80
C III] $\lambda 1908$	24.7	31.9	24.7	31.4	6.09	463	319	453	40.6	140
C II] $\lambda 2326$	6.20	9.46	*	*	*	*	16.5	26.0	14.9	68.9
[Ne IV] $\lambda 2423$	1.72	1.92	*	*	10.1 ^d	795	39.2	50.7	2.38	9.30
[O II] $\lambda 2470$	9.05	8.93	*	*	*	*	2.50	3.00	2.83	10.4

^a Notes: $F(\lambda)$ in units of $\text{erg cm}^{-2} \text{s}^{-1}$, $I(\lambda)$ in units such that $I(\text{H}\beta) = 100$. The quoted reddening constants are from the ratio of the 5 GHz free–free continuum to H β . For those PNe observed at ESO with a scanning slit the percentages of total nebular $F(\lambda 1640)$ in *IUE*'s large aperture are: 27% (NGC 2022), 60% (NGC 2440), 46% (NGC 3132), 53% (NGC 3242), 80% (NGC 3918), 65% (NGC 5882) and 48% (IC 4406);

^b From Clegg et al. (1987) combined with fluxes from spectrum SWP 47514;

^c From Feibelman (1998);

^d From Feibelman (2001);

^e From Hyung et al. (1999).

tained from the far-IR ratio (see Rubin 1989, Liu et al. 2001a). This effect will be discussed further in Section 5.2.

4.2 Electron temperatures

We derived T_e 's using ionic CEL ratios of nebular to transauroral [S II] transitions, nebular to auroral transitions of [N II], [O II] and [O III], and nebular to infrared fine-structure transitions of [O III] (the latter designated as $T_e(\text{O III})^{\text{IR}}$). We adopted the ISO Long Wavelength Spectrometer (LWS) fluxes listed by Liu et al. (2001) for the [O III] 52 μm and 88 μm lines. The LWS aperture size of ~ 80 arcsec included all of the emission from these nebulae. The results are presented in Table 7. We were able to derive values of $T_e(\text{O III})$ for all 15 PNe; values of $T_e(\text{N II})$ for 13 PNe, excluding SMC N87 and LMC N141 for which the auroral $\lambda 5754$ line did not fall within our wavelength coverage; and values of $T_e(\text{O III})^{\text{IR}}$ for eight PNe. The correct choice of electron temperature is crucial when deriving abundances from forbidden lines, so in what follows we discuss the pattern of T_e 's for the current sample of 15 PNe, as measured from the above ionic ratios.

4.2.1 Recombination excitation of the N II and O II auroral lines

The mean $T_e(\text{O III})$ for the whole sample is 12300 K, while the mean $T_e(\text{O II})$ is 11700 K. For 12 PNe where both T_e 's were measured, the values differ by about 3 per cent, $T_e(\text{O III})$ being only slightly higher than $T_e(\text{O II})$. It could be argued that generally in PNe, N $^+$ is present in a lower ionization zone than O $^{2+}$, and that the temperature should be lower too. However, for 8 PNe where both $T_e(\text{O III})$ and $T_e(\text{O II})$ can be measured, it is found that on average, $T_e(\text{O III}) = 11500$ K, while $T_e(\text{O II}) = 13400$ K, i.e. *higher* by 1900 K. The disagreement between [O II] and [O III] electron temperatures, as derived from the nebular to auroral line ratios $I(\lambda 3727)/I(\lambda 7320 + \lambda 7330)$ and $I(\lambda 4959 + \lambda 5007)/I(\lambda 4363)$, respectively, is at its most extreme in the cases of NGC 3242, NGC 5882 and My Cn 18. In these objects the derived $T_e(\text{O II})$'s are higher than the $T_e(\text{O III})$'s by 7850 K, 5900 K and 4980 K, respectively.

A variety of hypotheses can be invoked in order to explain the difference of electron temperatures in these three nebulae. Radiation hardening in the nebular volumes where singly ion-

Table 6. Electron densities.

PN	[O II] ^a $\lambda 3727/(\lambda 7320 + \lambda 7330)$	[S II] $\lambda 6731/\lambda 6716$	[Cl III] $\lambda 5537/\lambda 5517$	[Ar IV] $\lambda 4740/\lambda 4711$	[O III] ^b $52 \mu\text{m}/88 \mu\text{m}$
	$N_e (\text{cm}^{-3})$				
NGC 2022	1970	1050	850	2150	*
NGC 2440	*	*	*	4000	*
NGC 3132	*	550	720	530	355
NGC 3242	*	1970	1200	3040	775
NGC 3918	*	4600	5500	6900	1380
NGC 5315	13040	8200	22825	12300	2290
NGC 5882	4750	4000	2700	5000	1175
NGC 6302	5750	12900	22450	14900	1380
NGC 6818	1800	1700	2400	2350	*
IC 4191 ^c	13530	12750	12375	13750	*
IC 4191 ^d	11930	7900	10150	12800	1700
IC 4406	*	950	3500	1250	540
My Cn 18	*	5025	9420	6300	*
SMC N87	2850	3950	*	9500	*
LMC N66	≤ 200	1900	*	5700	*
LMC N141	2300	7400	*	9500	*

^a For NGC 5882, 6302, 6818 and LMC N66 quoted values were derived from the $\lambda 3729/\lambda 3726$ ratio;

^b From the *ISO* LWS line-fluxes of Liu et al. (2001);

^c Values from the fixed-slit spectrum of the nebula;

^d Values for the whole nebula from a scanned spectrum.

Table 7. Electron temperatures.

PN	[S II]	[O II]	[N II]	[O III]	$T_e (\text{K})$	BJ	[O III] ^{IR}	[O III] _{Cl III} ^{IR}	O II ORLs ^a
NGC 2022	*	*	14700	15000	13200	*	*	*	400
NGC 2440	*	*	*	16150	14000	*	*	*	*
NGC 3132	8120	*	9350	9530	10780	9900	9000	*	
NGC 3242	4800	19550	13400	11700	10200	13800	12400		1000
NGC 3918	9350	10400	10800	12600	12300	19900	12400		*
NGC 5315	11400	*	10800	9000	8600	18500	7800		8100
NGC 5882	6900	15300	10800	9400	7800	11400	9400		800
NGC 6302	10000	20200	14225	18400	16400	>50000	10900		*
NGC 6818	5750	11200	11100	13300	12140	*	*		$\lesssim 2900$
IC 4191 ^b	7750	*	11575	10700	10500	*	*		*
IC 4191 ^c	8550	*	12225	10000	9200	16700	8900		4300
IC 4406	8650	9000	9900	10000	9350	9900	7100		*
My Cn 18	12825	12300	10225	7325	*	*	*		*
SMC N87	>20000	*	*	12250	*	*	*		*
LMC N66	*	*	12700	18150	*	*	*		*
LMC N141	10100	*	*	11850	*	*	*		*

^a O II ORL temperatures from Paper II

^b Values from a fixed-slit spectrum of the nebula;

^c Values for the whole nebula from a scanned spectrum.

ized species are expected to exist, could result in higher temperatures than those of the O^{2+} zone, but the effect should be similar for both $T_e(\text{N II})$ and $T_e(\text{O II})$, since the ionization potentials of N^+ and O^+ are very comparable.

An alternative proposition is as follows: in NGC 3242,

NGC 5882 and My Cn 18 most of the N and O atoms are in their doubly ionized stages ($\text{O}^{2+}/\text{O} = 0.85, 0.96$ and 0.63 , while $\text{N}^{2+}/\text{N} = 0.65, 0.72$ and 0.63 , respectively; cf. Section 5). Thus, as discussed by Rubin (1986) and Liu et al. (2000), recombination of N^{2+} and O^{2+} can be important in contributing to the

excitation of the [N II] nebular and [O II] nebular and auroral lines.

We will attempt to quantify this effect for these three extreme cases, using the expressions of Liu et al. (2000). They employed radiative recombination coefficients from Péquignot, Petitjean & Boisson (1991) and dielectronic recombination coefficients from Nussbaumer & Storey (1984), to show that the intensity of the [N II] $\lambda\lambda 5754$ auroral line due to recombination excitation can be fitted by

$$\frac{I_R(\lambda 5754)}{I(H\beta)} = 3.19 t^{0.30} \times \frac{N^{2+}}{H^+}, \quad (1)$$

where $t \equiv T_e/10^4$ and $0.5 \leq t \leq 2.0$. Also, Liu et al. (2000) calculated new recombination coefficients for the metastable levels of O II and showed that the intensity of the [O II] $\lambda\lambda 7320, 7330$ auroral lines due to recombination excitation can be fitted in the range $0.5 \leq t \leq 1.0$ by

$$\frac{I_R(\lambda 7320 + \lambda 7330)}{I(H\beta)} = 9.36 t^{0.44} \times \frac{O^{2+}}{H^+}. \quad (2)$$

For NGC 3242, which has $T_e(O \text{ III}) = 11700 \text{ K}$, the observed $\lambda 1750$ multiplet flux yields $N^{2+}/H^+ = 1.90 \times 10^{-5}$, for $T_e = 11700 \text{ K}$ and $N_e = 1200 \text{ cm}^{-3}$ (Tables 6, 7). Inserting this value into Eq. 1, we have $I_R(\lambda 5754)/I(H\beta) = 0.0064$, or 10 per cent of the observed intensity of the $\lambda 5754$ line relative to $H\beta$, $I(\lambda 5754)/I(H\beta) = 0.0635$. After subtracting $I_R(\lambda 5754)$ from the observed intensity, the [N II] nebular to auroral line ratio yields $T_e = 10850 \text{ K}$, i.e. 2550 K lower than the value derived before the correction. If one uses instead $N^{2+}/H^+ = 1.28 \times 10^{-4}$, as derived from N II recombination lines (cf. Paper II for N^{2+}/H^+ and O^{2+}/H^+ abundances from N II and O II ORLs), one gets $I_R(\lambda 5754)/I(H\beta) = 0.0408$, which is about 64 per cent of the observed value. After correcting for this $I_R(\lambda 5754)$, the temperature deduced from the revised [N II] line ratio is only 7950 K.

Regarding the [O II] auroral lines, for $O^{2+}/H^+ = 2.80 \times 10^{-4}$ as derived from the $\lambda\lambda 4959, 5007$ lines (Table 9), Eq. 2 predicts a recombination intensity relative to $H\beta$ of 0.262 on a scale where $H\beta = 100$ for the [O II] $\lambda\lambda 7320, 7330$ lines, or 29 per cent of their observed intensity. According to Liu et al., the recombination contribution to the $\lambda\lambda 3726, 3729$ nebular lines is 7.7 times that of $I_R(\lambda 7320 + \lambda 7330)$, at $T_e = 10000 \text{ K}$. Thus we have, $I_R(\lambda 3726 + \lambda 3729) = 2.02$ on a scale where $H\beta = 100$, or 21 per cent of the observed overall intensity. Again, if we use instead the ORL abundance ratio of $O^{2+}/H^+ = 6.28 \times 10^{-4}$ derived for this PN, we get a recombination contribution of 0.588 to the [O II] auroral lines (65 per cent of the observed value), while a contribution of 4.53 relative to $H\beta$ (46 per cent of the observed intensity), is found for the nebular lines.

Therefore, using O^{2+}/H^+ as given by the CEL lines, the revised [O II] nebular to auroral line ratio yields $T_e = 15800 \text{ K}$, i.e. 3750 K lower than the value derived before the correction. If we instead use the O^{2+}/H^+ abundance ratio given by the ORLs, the corrected $T_e(O \text{ II})$ is 7500 K lower, at 12050 K, and only 300 K higher than the $T_e(O \text{ III})$.

Applying the same procedure to NGC 5882, which has $T_e(O \text{ III}) = 9400 \text{ K}$, we obtain from $N^{2+}/H^+ = 1.10 \times 10^{-4}$, as given by the CELs, a corrected nebular to auroral line ratio which yields a $T_e(N \text{ II})$ of 9900 K; if we assume $N^{2+}/H^+ = 1.63 \times 10^{-4}$, as given by the ORLs, the corrected temperature is $T_e(N \text{ II}) = 9550 \text{ K}$. Similarly, the corrected [O II] nebular to auroral line ratio results in a $T_e(O \text{ II})$ of 14500 K, us-

ing $O^{2+}/H^+ = 4.48 \times 10^{-4}$ as given by CELs; in the case of $O^{2+}/H^+ = 9.70 \times 10^{-4}$, as given by ORLs, the corrected temperature is $T_e(O \text{ II}) = 13750 \text{ K}$.

For My Cn 18, which has $T_e(O \text{ III}) = 7325 \text{ K}$, the [N II] line ratio does not change appreciably for $N^{2+}/H^+ = 2.20 \times 10^{-4}$ as given by CELs, so there is a negligible change in $T_e(N \text{ II})$; however if $N^{2+}/H^+ = 20.4 \times 10^{-4}$, as given by the ORLs, the corrected temperature becomes $T_e(N \text{ II}) = 9450 \text{ K}$. Finally, the corrected [O II] ratio results in a $T_e(O \text{ II})$ of 12150 K, using $O^{2+}/H^+ = 3.54 \times 10^{-4}$ as given by CELs; and for $O^{2+}/H^+ = 6.43 \times 10^{-4}$, as given by ORLs for this object, the corrected temperature is $T_e(O \text{ II}) = 12100 \text{ K}$.

In the above discussion we have neglected the contribution of recombination excitation to the observed [N II] $\lambda\lambda 6548, 6584$ nebular intensities; this is estimated to be small and amounts to only 7, 8 and 8 per cent, respectively, for NGC 3242, NGC 5882 and My Cn 18, even when adopting ORL N^{2+}/H^+ abundances. We base this on the fact that for pure recombination excitation, the [N II] nebular to auroral line ratio has a value of 5.9 at $T_e = 10000 \text{ K}$ (Liu et al. 2000). On the other hand, the observed ratios for these three PNe are respectively, 10, 12 and 13 times larger than that. We summarize our findings for these three objects in Table 8.

To conclude, for low-density uniform nebular media, as assumed above, appreciable fractions of the [O II] nebular and auroral and [N II] auroral lines can be accounted for by recombination processes. However, even after recombination excitation has been taken into account, the agreement between the various CEL temperature diagnostics remains quite poor, especially for NGC 5882 and My Cn 18 (see Table 8). In addition, the current treatment has not taken into account collisional de-excitation of the metastable levels that are populated by recombination. It is obvious that an exact analysis of this problem requires detailed knowledge of the actual electron temperature and N^{2+}/H^+ and O^{2+}/H^+ abundances. To complicate matters more, if the nebulae are not homogeneous, but also contain a higher-density component, then the observed [O II] and [N II] emission pattern can be more difficult to evaluate. In nebulae that contain condensations whose electron density is *higher* than the critical densities of the low-lying atomic levels—from which the $\lambda\lambda 6548, 6584$ and 3727 nebular lines originate—but *lower* than that of the auroral lines, the former lines will be preferentially emitted from the lower density medium. This could lead to apparently high temperatures as deduced from the [N II] and [O II] nebular to auroral ratios, since their component transitions would be disproportionately affected in regions of high density; there, the nebular lines will be suppressed by collisional de-excitation, but the auroral lines will not be (Viegas & Clegg 1994).

As our schematic treatment has pointed out, the [N II] and [O II] nebular to auroral temperature diagnostic ratios provide values which are probably poor indicators of T_e in the low-ionization regions of these three objects. Therefore, in the abundance analysis that follows in Section 7, we have adopted $T_e(O \text{ III})$ when calculating forbidden-line N^{+}/H^+ and O^{+}/H^+ abundances for NGC 3242, NGC 5882 and My Cn 18.

4.2.2 Balmer discontinuity electron temperatures

Apart from temperatures derived from the CEL ratios, Table 7 also lists the mean nebular Balmer jump temperatures, $T_e(BJ)$, derived from the ratio of the nebular continuum discontinuity

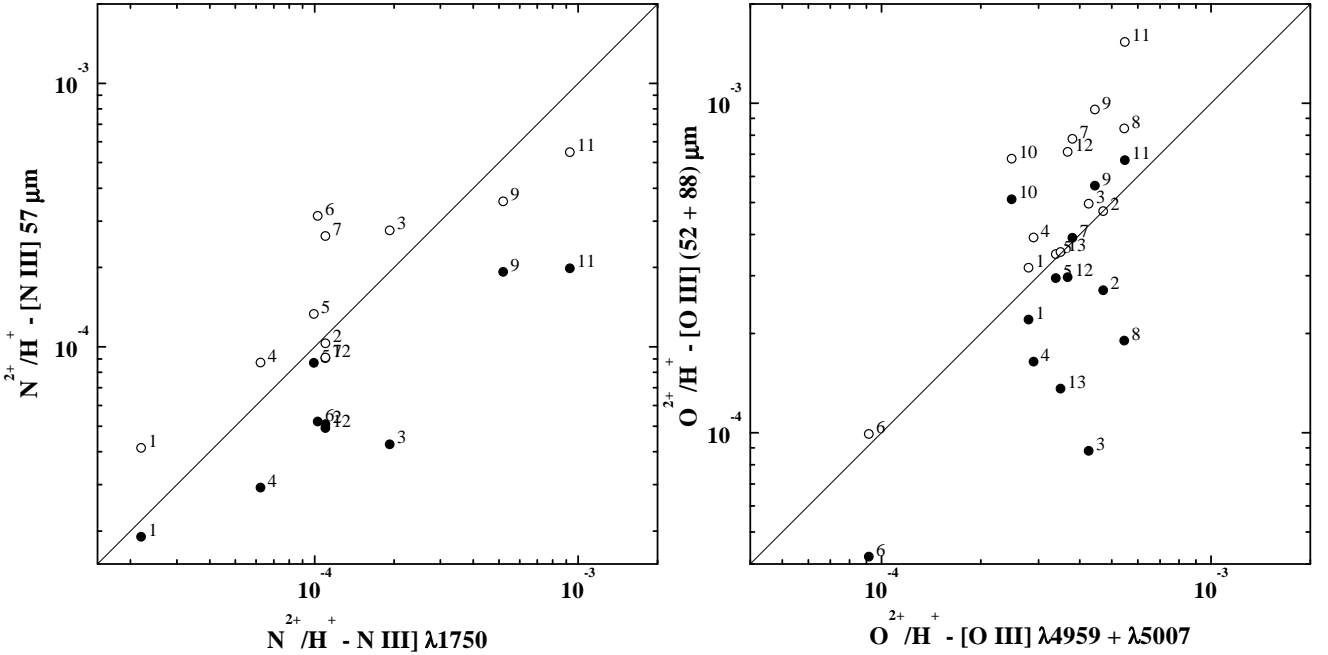


Figure 3. Comparison of N^{2+}/H^+ abundance ratios derived from the $N\text{ III}] \lambda 1750$ and $[N\text{ III}] 57\mu\text{m}$ lines, and O^{2+}/H^+ ratios derived from the $[O\text{ III}] \lambda\lambda 4959, 5007$ and $52, 88\mu\text{m}$ lines; solid and open circles denote abundances derived from adopting ‘low’ far-IR $[O\text{ III}] 88\mu\text{m}/52\mu\text{m}$ electron densities and ‘high’ $[\text{Cl III}], [\text{Ar IV}]$ electron densities, respectively; the data labelling refers to the designated PN numbers of Table 11, Col. 2.

vations. Table 6 compares the electron densities derived from the $88\mu\text{m}/52\mu\text{m}$ line ratio with those derived from the higher critical density $[\text{Cl III}]$, and $[\text{Ar IV}]$ ratios, for the eight PNe in common between our sample and Liu et al.’s (2001a) *ISO* LWS sample, and shows that on average the latter diagnostics yield N_e ’s about a factor of 6 higher than the far-IR ratio, confirming the existence of density inhomogeneities in these nebulae, in agreement with Liu et al.’s conclusions. In accord with the predictions of Rubin, the bias in the ionic N^{2+} and O^{2+} abundances derived from the far-IR lines becomes *less* when the higher electron densities from the $[\text{Cl III}]$ and $[\text{Ar IV}]$ are adopted – the values returned are then in good agreement, in most cases, with those derived from the $[N\text{ III}] \lambda 1750$ and $[O\text{ III}] \lambda\lambda 4959, 5007$ lines (cf. Table 9). For instance, in the case of NGC 5882 the ‘high’ density IR O^{2+} abundance is within 1 per cent of the optical CEL value, while the ‘high’ density IR N^{2+} abundance is within 7 per cent of the UV CEL value; in the case of NGC 3918, the UV N^{2+} and optical O^{2+} abundances agree to within 8 and 5 per cent with the corresponding values that are *half-way* between the listed IR abundances. A notable exception is IC 4406, for which the O^{2+}/H^+ abundance derived from the far-IR lines in the low density case agrees with the corresponding value derived from the optical lines. In Fig. 3 we plot abundance ratios of N^{2+}/H^+ and O^{2+}/H^+ derived from UV and optical lines respectively and compare them with those derived from far-IR transitions. Regarding the abundances from the IR lines, we plot using different symbols both those resulting from adopting the low $88\mu\text{m}/52\mu\text{m}$ ratio N_e ’s as well as those derived from adopting the higher $[\text{Cl III}], [\text{Ar IV}] N_e$ ’s. We see

that for the majority of nebulae very satisfactory agreement is found amongst the UV, and optical abundances on the one hand and the far-IR abundances on the other, after accounting for the modest density variations within the nebular volumes, exposed from the disparity between the IR and optical density diagnostic line ratios. In general, the adoption of electron densities just a little below those diagnosed by the $[\text{Cl III}]$ and $[\text{Ar IV}]$ ratios would lead to agreement between the abundances deduced from the infrared FS lines of $[O\text{ III}]$ and $[N\text{ III}]$ and those derived from the optical or UV lines of the same ions. These results are of importance in the context of the discussion about the existence of temperature fluctuations in nebulae and their potential impact on abundances derived from CELs (cf. Section 4.2.3).

We derived Ne^{2+}/H^+ abundances from the optical $[N\text{ III}] \lambda\lambda 3868, 3967$ lines for all 15 PNe. For 9 of them we also determined this abundance ratio using the *IRAS* $[N\text{ III}] 15.5\text{-}\mu\text{m}$ line fluxes of Pottasch et al. (1984). For the $15.5\text{-}\mu\text{m}$ line, $N_{cr} = 2 \times 10^5 \text{ cm}^{-3}$, and the resulting ionic abundances do not depend on the adopted N_e , for the range of nebular densities presented in Table 6. Inspection of Table 9 shows quite good agreement between the optical and infrared Ne^{2+}/H^+ abundances. As with other ions, the abundances from the optical CELs are those adopted.

In all these cases where IR collisionally excited lines were analyzed, we adopted the $T_e(O\text{ III})$ ’s for abundance determinations. IR CELs have small excitation energies, $E_{ex} < 1000\text{ K}$, much smaller than those of UV and optical forbidden lines. Thus their emissivities have only a weak dependence on the adopted nebular electron temperature, very similar to those of

H_I Balmer lines. Their intensities relative to H β are therefore virtually insensitive to the assumed temperature, unless the emitting medium has $T_e \ll 1000$ K; the electron temperatures of all nebulae in our sample, derived from CEL intensity ratios, are consistently much higher than that. On the other hand, at the temperatures implied by the O II ORLs (cf. Table 7 and Paper II) the far-IR CELs would be expected to be suppressed to various degrees depending on the exact temperature and density of the emitting material.

Ne³⁺/H⁺ ionic fractions were derived from the [Ne IV] $\lambda\lambda 4724, 4726$ and $\lambda 1601$ lines, which usually showed good agreement with each other. For the Ne⁴⁺/H⁺ ratio, whenever available the values obtained from [Ne V] $\lambda 3426$ were preferred over those from the Ne V $\lambda 1574$ line.

We adopted the S⁺/H⁺ abundance derived from the [S II] $\lambda\lambda 6716, 6731$ doublet, rather than from the transauroral $\lambda\lambda 4068, 4076$ lines, since the latter are potentially affected by recombination processes and density effects (the 2D and 2P atomic levels of S⁺, from which the $\lambda\lambda 6716, 6731$ and $\lambda\lambda 4068, 4076$ lines respectively arise, are directly analogous to the levels of O⁺ from which the [O II] nebular and auroral lines originate; especially in terms of critical densities).

5.3 Abundances – Summary

Table 11 presents total elemental abundances by number, expressed in units of $\log(X/H) + 12.0$, for X = He, C, N, O, Ne, S, Cl and Ar, for the 15 PNe analyzed in this work, plus the Galactic nebulae NGC 7009 (LSBC), NGC 6153 (Liu et al. 2000), and M 1-42 and M 2-36 (Liu et al. 2001b) which were previously observed in the context of our ongoing programme. Peimbert & Torres-Peimbert (1983) defined Type I PNe, believed to represent the high mass end of the PN distribution, as those having He/H ≥ 0.125 and N/O ≥ 0.5 by number. KB94 refined the Type I classification to refer to those PNe which have N/O ratios larger than the original (C + N)/O ratios of the parent galaxy ISMs out of which they formed, implying that any nitrogen in excess of this value must be primary in origin, e.g. via hot bottom burning of carbon brought up by the third dredge-up. For the Milky Way, the KB94 Type I criterion translates into N/O ≥ 0.74 . Using this, we classify NGC 2440, NGC 6302, NGC 7009 and M 1-42 as Type I. Table 11 also presents mean elemental abundances for the twelve non-Type I and four Type I Galactic PNe listed there and compares them with the mean non-Type I and Type I PN abundances of KB94, as well as with solar and M 42 (Orion Nebula) abundances. The mean N, O, Ne and S abundances for the twelve non-Type I Galactic PNe are slightly larger than the means found by KB94 for their larger sample of Galactic PNe. However, this may be because M 2-36, which has unusually large abundances for all elements, skews the mean values for our sample.

In Paper II we will use the much weaker heavy element optical recombination lines (ORLs) measured in the spectra reported here to derive ionic abundances and electron temperatures that can be compared with those derived in this paper from the CELs, in order to investigate whether our data replicate, and can throw light on, the significant discrepancies that have previously been found between CEL and ORL ionic abundances measured for a number of other planetary nebulae.

Acknowledgments

YGT acknowledges the award of a Perren studentship.

REFERENCES

- Allen C. W., 1973, Astrophysical Quantities. The Athlone Press, Univ. London
 Allende Prieto C., Lambert D. L., 2001, ApJ, 556, L63
 Allende Prieto C., Lambert D. L., 2002, ApJ, 573, L137
 Barlow M. J., 1987, MNRAS, 227, 161
 Burstein D., Heiles C., 1982, AJ, 87, 1165
 Cahn J. H., Kaler J. B., Stanghellini L., 1992, A&AS 94, 399 (CKS92)
 Clegg R. E. S., Harrington J. P., Barlow M. J., Walsh J. R., 1987, ApJ, 314, 551
 Dinerstein H. L., Lester D. F., Werner M. F., 1985, ApJ, 291, 561
 Esteban C., Peimbert M., Torres-Peimbert S., Escalante V., 1998, MNRAS, 295, 401
 Feibelman W. A., 1998, ApJ, 506, 773
 Grevesse N., Noels A., Sauval A. J., 1996, in Holt. S. S., Sonneborn G., eds, ASP Conf. Ser. Vol. 99, Cosmic Abundances, Astron. Soc. Pac., San Francisco, p. 117
 Henry R. B. C., Kwinter K. B., Bates J. A., 2000, ApJ, 531, 928
 Howarth I. D., 1983, MNRAS, 203, 201
 Hyung S., Aller L. H., Feibelman W. A., 1999, ApJ, 514, 878
 Kingsburgh R. L., Barlow M. J., 1994, MNRAS, 271, 257 (KB94)
 Kohoutek L., Laustsen S., 1977, A&A, 61, 761
 Kuhn H. G., 1969, Atomic Spectra (2nd ed., Longman)
 Kwok S., 1994, PASP, 106, 344
 Liu X.-W., 2002a, Rev. Mex. Astron. Astrof. (Ser. de Conf.), 12, 70
 Liu X.-W., 2002b, in Proc. IAU Symp. 209, Planetary Nebulae, ed. M. A. Dopita, Astron. Soc. Pac., San Francisco, in press
 Liu X.-W., Barlow M. J., Cohen M., Danziger I. J., Luo S.-G., Baluteau J. P., Cox P., Emery R. J., Lim T., Péquignot, D., 2001a, MNRAS, 323, 343
 Liu X.-W., Danziger I. J., 1993, MNRAS, 263, 256
 Liu X.-W., Luo S.-G., Barlow M. J., Danziger I. J., Storey P. J., 2001b, MNRAS, 327, 141
 Liu X.-W., Storey P. J., Barlow M. J., Clegg R. E. S., 1995, MNRAS, 272, 369 (LSBC)
 Liu X.-W., Storey P. J., Barlow M. J., Danziger I. J., Cohen M., Bryce M., 2000, MNRAS, 312, 585
 Luo S.-G., Liu X.-W., Barlow M. J., 2001, MNRAS, 326, 1049
 Milne D. K., Aller L. H., 1975, A&A, 38, 183
 Nussbaumer H., Storey P. J., 1984, A&AS, 56, 293
 Peimbert M., 1971, Bol. Obs. Tonantzintla y Tacubaya, 6, 29
 Pena, M., Ruiz M. T., 1988, RMxAA, 16, 55
 Péquignot D., Amara M., Liu X.-W., Barlow M. J., Storey P. J., Morisset C., Torres-Peimbert S., Peimbert M., 2002a, Rev. Mex. Astron. Astrof. (Ser. de Conf.), 12, 142
 Péquignot D., Liu X.-W., Barlow M. J., Storey P. J., Morisset C., 2002b, in Proc. IAU Symp. 209, Planetary Nebulae, ed. M. A. Dopita, Astron. Soc. Pac., San Francisco, in press
 Péquignot D., Petitjean P., Boisson C., 1991, A&A, 251, 680
 Prévot M. L., Lequeux J., Maurice E., Prévot L., Rocca-Volmerange B., 1984, A&A, 132, 389
 Rubin R. H., 1989, ApJS, 69, 897
 Rubin R. H., Simpson J. P., Haas M. R., Erickson E. F., 1991, ApJ, 374, 564
 Sahu K. C., Desai J. N., 1986, A&A, 161, 357
 Schachter J., 1991, PASP, 103, 457
 Storey P. J., Hummer D. G., 1995, MNRAS, 272, 41
 Tsamis Y. G., 2002, Ph.D. thesis, University of London
 Tsamis Y. G., Barlow M. J., Liu X.-W., Danziger I. J., Storey P. J., 2003a, MNRAS, 338, 687
 Tsamis Y. G., Barlow M. J., Liu X.-W., Storey P. J., Danziger I. J., 2003, MNRAS, submitted
 Peimbert M., Torres-Peimbert, S., 1983, in Proc. IAU Symp. 103 ‘Planetary Nebulae’, ed. D. R. Flower, Reidel. Dordrecht, p.233

- Viegas S., Clegg R. E. S., 1994, MNRAS, 271, 993
Walsh J. R., 1993, ST-ECF Newsletter, 19, 6
Zeippen C. J., 1982, MNRAS, 198, 111

APPENDIX A: ICF METHOD FOR THE DERIVATION OF C, N, AND O

Generally, in order to calculate total elemental abundances we made use of the *icf* scheme of KB94, with some modifications in those cases *only* where our observations of heavy-element optical recombination lines (and the resultant ORL abundances; Paper II) enabled us to account in a satisfactory manner for missing ionic stages. Below we describe how we derived the *icfs* for C, N, and O from this method.

NGC 2022: In the case of carbon we use the standard KB94 correction factor $1 + O^{+}/O^{2+}$ to account for missing C^{+} , while from the ratio C^{4+}/C^{3+} as derived from ORLs and the CEL C^{3+} abundance we estimate $C^{4+}/H^{+} = 5.53 \times 10^{-5}$ [thus $icf(C) = 1.02$]. For N, we use the ratio N^{4+}/N^{3+} as derived from ORLs and the CEL N^{3+} abundance to estimate $N^{4+}/H^{+} = 2.35 \times 10^{-6}$ [thus $icf(N) = 1.09$]. Similarly for O, we estimate $O^{4+}/H^{+} = 8.69 \times 10^{-5}$ from the O^{4+}/O^{3+} ratio derived from ORLs and the CEL O^{3+} abundance [thus $icf(O) = 1.24$].

NGC 2440: We treat C exactly as in the case of NGC 2022, using the standard correction for C^{+} and estimating $C^{4+}/H^{+} = 3.77 \times 10^{-5}$ with the help of the ORL C^{4+}/C^{3+} ratio and the CEL C^{3+} abundance [thus $icf(C) = 1.89$]. Our C abundance is only 2 per cent higher than the one found if we follow the standard *icf* scheme based on nitrogen. For nitrogen, we make use of the CEL N^{+}/N^{2+} ratio given by KB94 and our own N^{2+} abundance to estimate $N^{+}/H^{+} = 3.37 \times 10^{-5}$ [thus $icf(N) = 1.31$]. For oxygen, since our spectral coverage of the nebula did not allow the derivation of an O^{+} abundance, we made use of the CEL ratio O^{+}/O^{2+} from Liu & Danziger (1993; from their 270 deg. slit), along with our O^{2+} abundance to estimate $O^{+}/H^{+} = 2.76 \times 10^{-5}$. We also estimate $O^{4+}/H^{+} = 3.43 \times 10^{-5}$ using our ORL ratio O^{4+}/O^{3+} and the CEL O^{3+}/H^{+} abundance ratio [thus $icf(O) = 1.34$].

NGC 3132: The standard schemes were used in the case of C and O, while for nitrogen we use our ORL N^{3+}/N^{2+} ratio and the CEL N^{2+} abundance to estimate $N^{3+}/H^{+} = 7.22 \times 10^{-6}$ [thus $icf(N) = 1.03$].

NGC 3242: For C and O we used the standard scheme, while for nitrogen using our ORL N^{3+}/N^{2+} ratio and the CEL N^{2+} abundance we find $N^{3+}/H^{+} = 1.18 \times 10^{-5}$ [thus $icf(N) = 1.53$].

NGC 3918: For N and O we follow the standard scheme, while for carbon we use the ratio C^{4+}/C^{3+} as derived from ORLs and the CEL C^{3+} abundance to estimate $C^{4+}/H^{+} = 2.62 \times 10^{-5}$ [thus $icf(C) = 1.06$].

NGC 5315: For N and O we follow the standard scheme, while for carbon we use our ORL C^{3+}/C^{2+} ratio and the CEL C^{2+} abundance to estimate $C^{3+}/H^{+} = 4.61 \times 10^{-6}$ [thus $icf(C) = 1.02$].

NGC 5882: For O we used the standard scheme; for carbon we estimate $C^{3+}/H^{+} = 1.81 \times 10^{-5}$ from the ORL C^{3+}/C^{2+} ratio and the CEL C^{2+} abundance [thus $icf(C) = 1.17$]. For nitrogen we use our ORL N^{3+}/N^{2+} ratio and the CEL N^{2+} abundance to estimate $N^{3+}/H^{+} = 3.88 \times 10^{-6}$ [thus $icf(N) = 1.35$].

NGC 6818: For carbon we used the ratio C^{4+}/C^{3+} as derived from ORLs and the CEL C^{3+} abundance to estimate

$C^{4+}/H^{+} = 7.20 \times 10^{-6}$ [thus $icf(C) = 1.03$]. For N we used the standard scheme, while for oxygen we use our ORL ratio O^{4+}/O^{3+} and the CEL O^{3+} abundance to estimate $O^{4+}/H^{+} = 4.97 \times 10^{-5}$ [thus $icf(O) = 1.11$].

IC 4191: We used the standard scheme for C and O, whereas for nitrogen we used our ORL N^{3+}/N^{2+} ratio and the CEL N^{2+} abundance to estimate $N^{3+}/H^{+} = 4.80 \times 10^{-6}$ [thus $icf(N) = 1.14$].

IC 4406: We used the standard scheme for C and O, whereas for nitrogen we used our ORL N^{3+}/N^{2+} ratio and the CEL N^{2+} abundance to estimate $N^{3+}/H^{+} = 4.23 \times 10^{-5}$ [thus $icf(N) = 1.25$].

Finally, for NGC 6302, My Cn 18, SMC N87, LMC N66 and LMC N141 we used the standard scheme throughout.

Table 3. –continued

λ_{obs}	My Cn 18				
	$F(\lambda)$	$I(\lambda)$	ID	λ_0	Mult
$c(\text{H}\beta)^{\text{Ba}} = 1.24$					
6547.09	1.43(+2)	5.79(+1)	[N II]	6548.10	F1
6561.75	5.73(+2)	2.29(+2)	H 3	6562.77	H3
6582.48	4.42(+2)	1.76(+2)	[N II]	6583.50	F1
6677.03	9.92	3.79	He I	6678.16	V46
6715.42	7.58	2.86	[S II]	6716.44	F2
6729.80	1.34(+1)	5.04	[S II]	6730.82	F2
7063.98	1.54(+1)	5.11	He I	7065.25	V10
7134.51	3.43(+1)	1.10(+1)	[Ar III]	7135.80	F1
7176.65	1.01	3.23(−1)	He II	7177.50	5.11
7230.02	2.47(−1)	7.71(−2)	C II	7231.32	V3
7235.12	6.20(−1)	1.93(−1)	C II	7236.42	V3
7279.85	1.65	5.08(−1)	He I	7281.35	V45
7318.18	1.19(+1)	3.61	[O II]	7318.92	F2
7328.93	1.00(+1)	3.02	[O II]	7329.67	F2

Table 4. Observed and dereddened relative line fluxes [$F(\lambda)$ and $I(\lambda)$, respectively], on a scale where $\text{H}\beta = 100$.

λ_{obs}	SMC N87				
	$c(\text{H}\beta)^{\text{Ba}} = 0.03 \text{ (Gal)}, 0.02 \text{ (SMC)}$				
$c(\text{H}\beta)^{\text{Ba}} = 0.03 \text{ (Gal)}, 0.02 \text{ (SMC)}$					
1549	49.7	62.4	C IV	1549	
1663	19.3	23.8	O III]	1663	
1908	451	550	C III]	1908	
2426	52.1	62.4	C II]	2426	
3721.72	1.26	1.61	H 14	3721.94	H14
*	*	[S III]	3721.63	[S III]	
3725.79	3.74	4.79	[O II]	3726.03	F1
3728.58	2.14	2.73	[O II]	3728.82	F1
3734.06	9.41(−1)	1.20	H 13	3734.37	H13
3749.98	1.41	1.79	H 12	3750.15	H12
3770.46	1.52	1.93	H 11	3770.63	H11
3797.73	2.39	3.00	H 10	3797.90	H10
3835.22	3.83	4.76	H 9	3835.39	H9
3868.47	1.70(+1)	2.10(+1)	[Ne III]	3868.75	F1
3888.77	1.00(+1)	1.22(+1)	He I	3888.65	V2
3967.17	6.55	7.88	[Ne III]	3967.46	F1
3969.78	9.71	1.16(+1)	H 7	3970.07	H7
4025.99	1.91	2.26	He I	4026.21	V18
4070.30	3.08(−1)	3.61(−1)	[S II]	4068.60	F1
4071.46	1.45(−1)	1.71(−1)	O II	4069.62	V10
*	*	O II	4069.89	V10	
4073.86	5.52(−2)	6.48(−2)	O II	4072.16	V10
*	*	O II	4075.86	V10	
4078.06	1.39(−1)	1.63(−1)	[S II]	4076.35	F1
4080.55	2.29(−2)	2.69(−2)	O II	4078.84	V10
4086.82	3.09(−2)	3.61(−2)	O II	4083.90	V48b
4088.03	1.08(−2)	1.27(−2)	O II	4085.11	V10
4090.07	2.45(−2)	2.86(−2)	O II	4087.15	V48c
*	*	O II	4089.29	V48a	
4103.46	2.28(+1)	2.65(+1)	H 6	4101.74	H6
*	*	O II	4120.54	V20	
4122.46	2.59(−1)	3.01(−1)	He I	4120.84	V16
4145.37	3.09(−1)	3.56(−1)	He I	4143.76	V53
4188.46	9.46(−2)	1.08(−1)	C III	4186.90	V18
4268.66	5.98(−1)	6.72(−1)	C II	4267.15	V6
4294.11	4.16(−2)	4.65(−2)	O II	4292.21	V78c
4327.58	5.66(−2)	6.27(−2)	O II	4325.76	V2
4342.02	4.20(+1)	4.64(+1)	H 5	4340.47	H5
4351.07	4.53(−2)	5.00(−2)	O II	4349.43	V2
4359.53	3.54(−2)	3.89(−2)	O II	4357.25	V63a
4364.79	6.16	6.78	[O III]	4363.21	F2
4389.55	5.70(−1)	6.23(−1)	He I	4387.93	V51
4439.03	1.15(−1)	1.24(−1)	He I	4437.55	V50
4458.31	2.33(−2)	2.51(−2)	Ne II	4457.24	V61d
4473.10	4.96	5.33	He I	4471.50	V14
4641.10	7.99(−2)	8.32(−2)	O II	4638.86	V1
4643.26	1.29(−2)	1.34(−2)	N III	4640.64	V2
4644.06	7.99(−2)	8.31(−2)	O II	4641.81	V1
4649.59	7.52(−2)	7.81(−2)	C III	4647.42	V1
4651.30	7.52(−2)	7.81(−2)	O II	4649.13	V1
4652.42	4.51(−2)	4.68(−2)	C III	4650.25	V1
4653.01	7.52(−2)	7.81(−2)	O II	4650.84	V1
4653.64	1.50(−2)	1.56(−2)	C III	4651.47	V1
4675.16	7.95(−3)	8.25(−3)	[Fe III]	4658.10	F3
*	*	C IV	4658.30	V8	
4677.67	2.34(−2)	2.43(−2)	O II	4661.63	V1
4677.66	2.40(−2)	2.48(−2)	O II	4676.24	V1
4713.41	2.65(−1)	2.72(−1)	[Ar IV]	4711.37	F1
4715.22	9.08(−1)	9.32(−1)	He I	4713.17	V12
4742.22	3.97(−1)	4.05(−1)	[Ar IV]	4740.17	F1
4755.96	2.78(−2)	2.83(−2)	[Fe III]	4754.83	
4758.33	1.34(−2)	1.37(−2)	?		
4802.77	2.80(−2)	2.83(−2)	?		

Table 11. Elemental abundances relative to H derived from CELs, except for the helium abundances which are from ORLs, in units where $\log N(H) = 12.0$.^a

PN	No.	He	C	N	O	Ne	S	Cl	Ar
NGC 2022		11.04	8.33	7.46	8.66	7.84	6.57	4.91	6.12
NGC 2440 (I)		11.08	8.37	8.26	8.39	8.04	*	*	*
NGC 3132	(5)	11.08	8.50	8.37	8.82	8.49	7.03	5.36	6.73
NGC 3242	(1)	11.00	8.14	7.53	8.52	7.89	6.38	4.94	5.99
NGC 3918	(4)	11.00	8.64	8.02	8.86	7.97	6.70	5.11	6.24
NGC 5315	(3)	11.08	8.33	8.52	8.79	8.30	7.31	5.41	6.56
NGC 5882	(2)	11.04	8.18	8.18	8.67	8.13	6.92	5.26	6.31
NGC 6153 ^b	(9)	11.14	8.44	8.36	8.70	8.23	7.21	5.62	6.43
NGC 6302 (I)	(6)	11.13	7.89	8.52	8.40	7.88	6.75	4.99	6.34
NGC 6818		11.00	8.41	7.74	8.71	8.07	6.56	5.09	5.94
NGC 7009 ^c (I)	(12)	11.04	8.66	8.50	8.61	8.24	6.98	*	6.27
IC 4191	(8)	11.08	*	7.59	8.78	8.21	7.10	5.37	6.49
IC 4406	(7)	11.09	8.56	8.32	8.76	8.33	6.33	5.16	6.40
My Cn 18		10.99	*	8.34	8.75	8.09	7.24	5.39	*
M 1-42 ^d (I)	(10)	11.17	7.80	8.68	8.63	8.12	7.08	5.26	6.56
M 2-36 ^d	(11)	11.13	8.73	8.42	8.85	8.57	7.47	5.42	6.66
Mean non-Type I		11.06	8.46	8.30	8.75	8.23	7.04	5.30	6.37
Mean Type I		11.11	8.32	8.51	8.52	8.09	6.96	5.15	6.41
KB94 non Type-I ^e		11.05	8.81	8.14	8.69	8.10	6.91	*	6.38
KB94 Type-I ^e		11.11	8.48	8.72	8.65	8.09	6.91	*	6.42
Solar ^f		10.99	8.39	7.97	8.69	8.09	7.21	5.50	6.56
M 42 ^g		10.99	8.53	7.78	8.52	7.89	7.17	5.33	6.80
SMC N87		10.99	8.58	7.55	8.03	7.03	*	*	5.32
LMC N66		11.02	7.52	7.99	8.50	7.62	6.63	*	6.10
LMC N141		11.04	8.30	7.95	8.29	7.38	6.61	*	5.88

^a Values are for the whole nebulae, except NGC 6302, 6644, 6572, 6818, 7009, My Cn 18, IC 4406, LMC N66 and M 42, where values are from fixed-slit spectra. A “(I)” after a PN’s name indicates that it is a Type I nebula (see text).

^b From Liu et al. (2000).

^c From LSBC for He & O; Henry, Kwitter & Bates (2000) for C & N; Luo, Liu & Barlow (2001) for Ne; KB94 for S & Ar.

^d From Liu et al. (2001b).

^e From KB94 mean abundances.

^f Solar photospheric abundances from Grevesse et al. (1996), except C and O which are from Allende Prieto et al. (2001, 2002).

^g CEL abundances for M 42 from Esteban et al. (1998), except O, which is from our unpublished ESO 1.52-m and AAT 3.9-m data, and C, which is from Rubin et al. (1991).